iScience

CellPress
OPEN ACCESS

Article

Lupeol synergizes with 5-fluorouracil to combat c-MET/EphA2 mediated chemoresistance in triple negative breast cancer

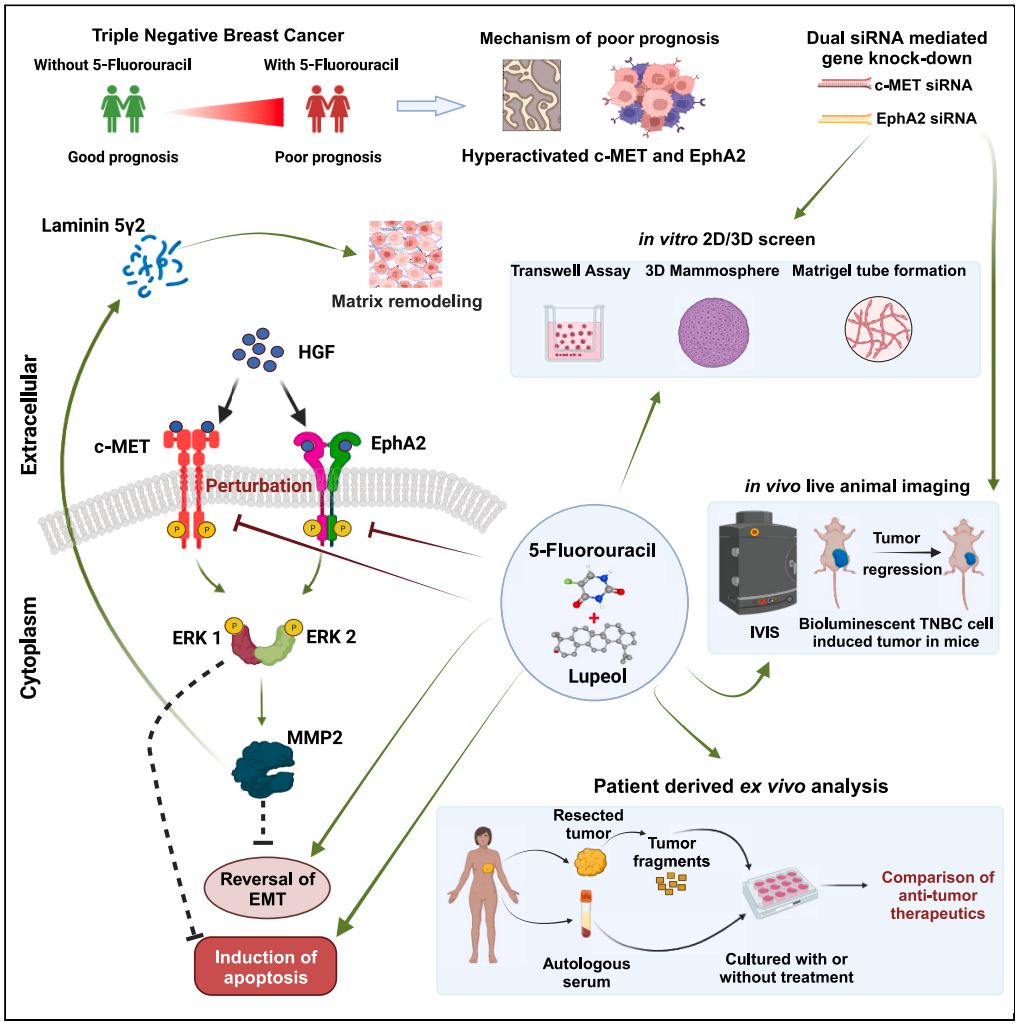

Debarpan Mitra, Depanwita Saha, Gaurav Das, ..., Anuj Majumder, Biswanath Majumder, Nabendu Murmu

nabendu.murmu@cnci.ac.in

Highlights

5FU based treatment modalities show relatively poor prognosis in TNBC

c-MET and EphA2 display hyperactivation in patients with 5FU driven chemotherapy

Dual silencing of *c-MET* and *EphA2* decreases tumorigenic potential of TNBC cells

Synergism of Lupeol and 5FU elicits anti-TNBC effects *in vitro, in vivo and ex vivo*

Mitra et al., iScience *26*, 108395
December 15, 2023
https://doi.org/10.1016/j.isci.2023.108395

iScience

CellPress
OPEN ACCESS

Article

Lupeol synergizes with 5-fluorouracil to combat c-MET/EphA2 mediated chemoresistance in triple negative breast cancer

Debarpan Mitra,[1] Depanwita Saha,[1] Gaurav Das,[1] Rimi Mukherjee,[1] Samir Banerjee,[1] Neyaz Alam,[2] Saunak Mitra Mustafi,[3] Partha Nath,[2] Anuj Majumder,[4,5] Biswanath Majumder,[6,7] and Nabendu Murmu[1,8,*]

SUMMARY

Triple-negative breast cancer (TNBC) is the most elusive subtype of breast cancer that encounters treatment dilemmas owing to the paucity of druggable targets. We found hyperactivation of c-MET and ephrin type-A receptor 2 (EphA2) in patients treated with 5FU driven chemotherapy which correlated with lower disease-free survival. However, silencing of both these genes resulted in a marked decrease in the invasive, migratory, and tumorigenic potential of TNBC cells, indicating that a dual target strategy is actionable. Lupeol is a phytochemical, with potent anticancer efficacy and minimal side effects in preclinical studies. A synergistic strategy with 5FU and Lupeol elicited promising anticancer responses *in vitro*, *in vivo*, and in patient-derived *ex vivo* tumor culture models. This synergistic regimen is effective, even in the presence of HGF, which mechanistically orchestrates the activation of c-MET and EphA2. These data lay the foundation for the clinical validation of this combination therapy for TNBC patients.

INTRODUCTION

Breast cancer is currently the most commonly diagnosed cancer worldwide and the 5th leading cause of cancer-related deaths due to cancer.[1] Approximately 10–20% of all breast cancers are found to be triple negative breast cancer (TNBC) subtype, which is often associated with very poor prognosis even at early stages of the disease. Over the last few decades, enormous efforts have been made to understand the underlying molecular mechanisms and improve the clinical scenario, including new molecular subtypes and new generation therapeutic modalities. However, overall survival (OS) remains low.[2]

Among the conventional therapies, the National Comprehensive Cancer Network (NCCN) guidelines recommend using combination regimens based on cyclophosphamide, anthracycline, taxane, fluorouracil, and cisplatin.[3] Unfortunately, all these drugs have severe adverse effects while conferring low and temporary responses. Fluorouracil, despite being an important component of chemotherapy regimens, is more likely to cause nausea, myelosuppression, and ovarian failure.[4] Moreover, not all individual agents in combination chemotherapy uniformly and consistently exert anticancer cytotoxic responses in a synergistic fashion for all patients where regimens show clinical benefits.[5,6] With these existing challenges, there is an urgent unmet need for the development of more effective and affordable drug combinations that have bearable side effects and, at the same time, durable and deep responses against TNBC and other similar molecular subtypes. Elucidation of viable TNBC targets is an obstacle that needs to be overcome. c-MET (mesenchymal-epithelial transition factor) and ephrin type-A receptor 2 (EphA2) may be considered two of such druggable targets for exploring novel therapeutic opportunity in case of TNBC, as these receptor tyrosine kinases (RTKs) show robust expression in this subset of breast cancer.[7–9]

The hepatocyte growth factor receptor (HGFR), also known as c-MET, is an RTK encoded by *c-MET* gene. Aberrant c-MET signaling has been mechanistically linked to the promotion of breast cancer, and its contextual dysfunction represents an aggressive phenotype.[10] Among all breast cancers, c-MET is over-expressed in 20%–30% of the cases and is more prevalent in TNBC, where 52% of patient tumors express this critical alteration. Drugs that target the oncogenic c-MET pathway are effective against many cancers, including TNBC. Indeed, to maximize anti-c-MET efficacy in personalized settings, further trial designs based on biomarker-guided patient stratification are part of a smart and rational combination selection approach.[11,12] The downstream effect of c-MET activation relies on canonical

[1]Department of Signal Transduction and Biogenic Amines, Chittaranjan National Cancer Institute, 37, S. P. Mukherjee Road, Kolkata 700026, India
[2]Department of Surgical Oncology, Chittaranjan National Cancer Institute, 37, S. P. Mukherjee Road, Kolkata 700026, India
[3]Department of Pathology, Chittaranjan National Cancer Institute, 37, S. P. Mukherjee Road, Kolkata 700026, India
[4]Department of Medicine, Harvard Medical School, 65 Lansdowne Street, Suite #317, Cambridge, MA 02139, USA
[5]Brookline High School, 115 Greenough Street, Brookline, MA 02445, USA
[6]Departments of Molecular Profiling, Cancer Biology and Molecular Pathology, Mitra Biotech, Bangalore, India
[7]Present address: Oncology Division, Bugworks Research, C-CAMP, Bangalore, India
[8]Lead contact
*Correspondence: nabendu.murmu@cnci.ac.in
https://doi.org/10.1016/j.isci.2023.108395

signaling modulators that are common in many RTKs, and mechanistically include activation of the nodal mitogen-activated protein kinase (MAPK) cascades[13,14] which contextually induces the degradation of matrix proteins, promotion of cell migration, and sustained tumor proliferation.[15,16]

In a complex interactive RTK network, EphA2 is another complementary oncoprotein that is over-expressed in human breast tumors and associated with poor prognosis.[17] From these perspectives, like c-MET, oncogenic EphA2 may underpin critical dysregulation and may act as a clinically actionable driver, influencing the clinical progression of TNBC and may further facilitate angiogenesis, migration, invasion/metastasis, and eventual treatment resistance. Preclinical evidence supporting this hypothesis revealed that, in MDCK cells, hepatocyte growth factor (HGF), upon binding to its cognate receptor c-MET, leads to the activation of EphA2 at the S897 residue, which is a non-canonical form of activation for this receptor.[18] Phosphorylation of EphA2 at this specific residue in breast cancer patients leads to reduced OS and disease-free survival (DFS) and has the potential to act as an independent prognostic indicator.[19] Both c-MET and EphA2 receptors respond to HGF-mediated activation and involve the downstream activation of a number of effector molecules, leading to similar phenotypic modulations. From these perspectives, we explore the mechanistic link that implicates this activation in 5FU refractory TNBC and further interrogate the novel combination that appreciates these phenotypes as a therapeutic vulnerability in TNBC. We tested the impact of individual as well as paired silencing of the aforementioned RTKs in an *in vitro* and *in vivo* setting.

Plant-derived small molecules are used in many clinical indications, including cancer. Lupeol, a pentacyclic triterpenoid, is a natural product that exhibits biological activity against cancer.[20–25] Since Lupeol has the potential to act as a synergy partner for chemotherapeutic drugs used for the treatment of breast cancer,[26] we evaluated 5FU with Lupeol for their ability to cf. pharmacological perturbation of TNBC in the context of therapeutic vulnerability using *in vitro* and syngeneic mice model and expanded the results inpatient derived *ex vivo* tumor fragment culture.

RESULTS

5-Fluorouracil non-response and delineation of its underlying mechanism

From our follow up study and the Kaplan-Meier plot for DFS (Figure 1A), it was observed that there was a significant difference (log rank [Mantel-Cox] = 4.405; p = 0.036) in DFS between the cohort that received 5FU containing standard of care (SOC) and the cohort that received other SOC not containing 5FU. The actual screening method, along with the exclusion and inclusion criteria during patient selection, is shown in Figure S1. The TNBC patient cohort details are shown in Table S1 (N = 135) and (N = 15) Table S2 for the *ex vivo* tumor fragment culture. The mean (95% Confidence Interval) DFS time of patients who received 5FU SOC was 49.517 $\pm$ 3.302 months (43.045–55.988) and that of other SOC was 58.982 $\pm$ 3.210 months (52.690–65.274). Archived tumor blocks of recurrent tissues were collected and probed for the phosphorylation status of EphA2 and c-MET (Figure 1B), these two RTKs have been extensively implicated in drug resistance, poor patient prognosis, and survival in various cancer models, including TNBC.[7,9,17,19,27–29] Notably, both EphA2 (p = 0.001) and c-MET (p = 0.032) were significantly more phosphorylated in the 5FU based SOC treated cohort (Tables S3 and S4). Next, fresh TNBC samples were collected and cultured for 48 h under sterile conditions, and the samples were exposed to 5FU in the presence of HGF (Figure 1C). Subsequently, tumor blocks were prepared by probing for Ki67 and Caspase 3c revealed two distinct cohorts. The cohort where there was a significant difference in the expression patterns of Ki67/Caspase 3c among the various treatment arms were designated as the "responders" (Figure 1D) and where there was no significant difference were the "non-responders" (Figure 1E). Furthermore, we checked for the phosphorylation status of EphA2 and c-MET and found that they were significantly more phosphorylated in the non-responders even after exposing the tissue to 5FU (Figure 1F) (Tables S5 and S6). This sheds light on the underlying mechanism of treatment failure and non-response to 5FU containing SOC, and the activated status of EphA2 and c-MET in the presence of HGF may be implicated in the same. Graphs representing the IHC scores vs. the various treatment arms are shown in Figure S2.

Dual knockdown of c-MET and EphA2 signaling exhibits reversal of phenotype in TNBC cells

Prior evidence highlighting that both c-MET and EphA2 surface receptors are upregulated in TNBC cells provides a suitable model for evaluating the potential crosstalk between these receptor signaling pathways.[30–32] To investigate the possible crosstalk between the c-MET and EphA2 signaling axes in TNBC cells, we utilized siRNA-mediated silencing of targets in both MDA-MB-231 and 4T1 cell lines. Upon transfecting the cells with various concentrations of the siRNA, maximum inhibition of protein expression was demonstrated at 150 nM concentration of both c-MET and EphA2 siRNAs in both cell lines (Figure S3). Additionally, specific phospho-c-MET inhibitors (cabozantinib) and phospho-EphA2 inhibitors (ALW-II-41-27) were used as pharmacological antagonists. A dual silencing strategy was adopted in which the cells were subjected to concurrent knockdown of c-MET and EphA2. In parallel, cells were treated with c-MET and EphA2 inhibitors together in a separate group. All groups, apart from the control groups (vehicle control and non-targeting pool [NTP] as negative control), were subsequently treated with HGF (100 ng/mL) for 15 min prior to cell lysate preparation. Western blot analysis revealed that HGF induced phosphorylation of both c-MET and EphA2 receptors and resulted in the upregulation/activation of key downstream molecules, namely, phospho-ERK1/2, MMP2, and Laminin-5γ2 (Figure 2A). Notably, phosphorylation of EphA2 was specifically detected at S897, a selective kinase active site that has been implicated in promoting tumorigenic activity and activation of the ERK1/2 cascade, leading to increased cellular plasticity, ECM remodeling, and evasion of apoptosis.[18,33] Upon individual knockdown of either c-MET or EphA2 in the presence of HGF, the residual constitutive expression of downstream molecules was observed. This tonic signal was entirely abolished in the dual knockdown and inhibitor groups, suggesting the presence of a compensatory downstream cascade. Further ascertaining the functional consequences of this perturbation, dual knockdown groups displayed maximum potency in preventing cellular

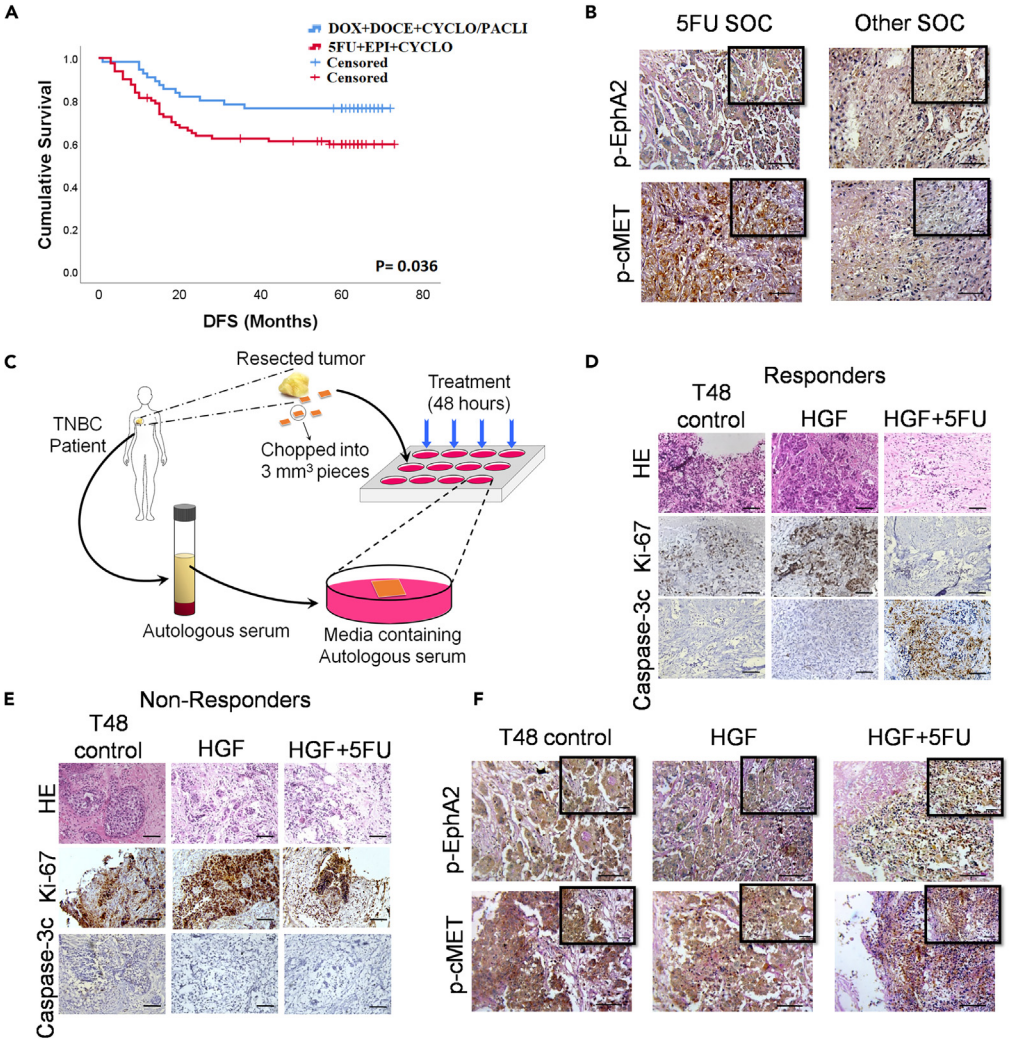

Figure 1. Treatment failure and evaluation of the underlying mechanism of non-response in TNBC recurrence, post treatment with 5FU

(A) Survival curve of DFS in TNBC patients with differential treatment regimens, one SOC containing 5FU and the other cohort received SOC without 5FU.

(B) Differential expression of phospho-EphA2 and phospho-*c*-MET in recurrent TNBC tissue.

(C) Schematic representation of *ex vivo* explants culture.

(D and E) Differential expression of Ki67 and Caspase 3c in TNBC patient derived *ex vivo* explants cultures, stratifying the cohort into responders and non-responder population.

(F) Expressional status of phopsho-EphA2 and phospho-*c*-MET in the non-responder population from explants cultured tissues. Data are representative of triplicate experiments. *p < 0.05 represents statistically significant difference and was calculated by the log-rank test. Scale bars: 200 μm and 100 μm (in inset). HGF = hepatocyte growth factor; 5FU = 5-fluorouracil; SOC = standard of care; TNBC = triple negative breast cancer; HE = Hematoxylin & Eosin staining. Also see, Figures S1 and S2; Tables S1–S6.

migration and invasion when compared to individual knockdown groups in the presence of HGF (Figures 2B and 2C; Figures S4A and S4B). A schematic diagram of the mammosphere formation assay is shown in Figure 2D. Similar effects were observed in the mammosphere and Matrigel tube formation assays upon HGF treatment in cells with complete knockdown or inhibition (Figures 2E and 2F; Figures S4C and S4D). The relative mammosphere formation efficiency was compromised in the dual knockdown groups, indicating that inhibiting only the c-MET or EphA2 axis in the presence of HGF is not sufficient to completely abrogate sphere formation. Similarly, the total number of intracellular junctions and the total vessel length drastically reduced as the cells were impaired to form proper tube-like structures in Matrigel in the dual knockdown groups, compared to individual knockdown groups (Figures S4E and S4F.). These findings were further validated in a TNBC syngeneic mouse model, wherein c-MET, EphA2, or dual knockdown 4T1 cells were injected into the mammary fat pads of BALB/c mice. Subsequently, the mice were exposed to HGF. The tumor volume was significantly lower in the dual knockdown group (Figures 2G and 2H), thus confirming that dual targeting of c-MET and EphA2 has a more significant impact on abrogating tumorigenesis in TNBC cell populations.

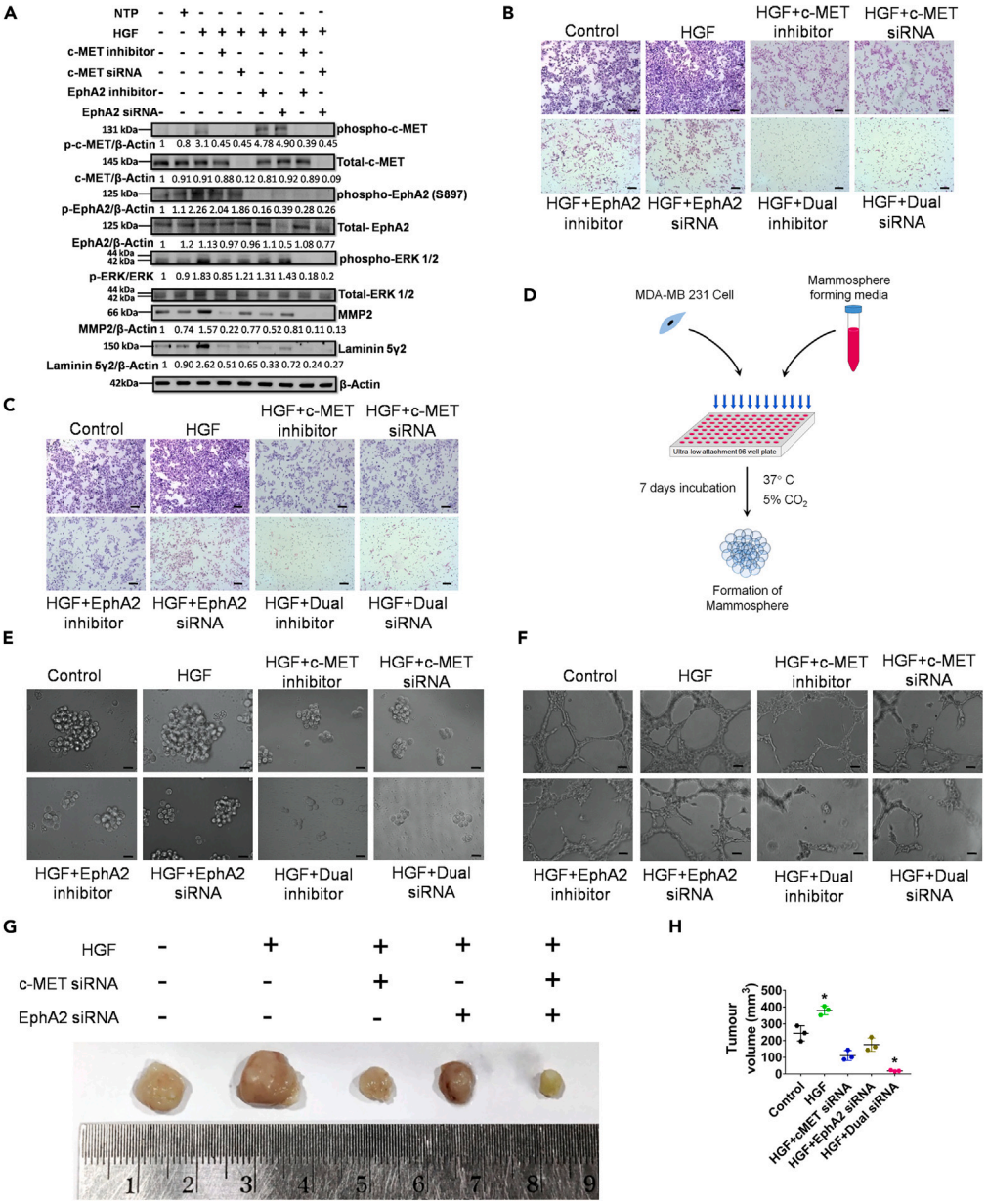

Figure 2. Evaluation of the effect of individual and dual knock down of c-MET and EphA2 genes on MD-MB-231 in the presence of HGF

(A) c-MET and EphA2 knockdown/inhibition and its effect on downstream effectors on MDA-MB-231 cells was analyzed by western blot; NTP = non-target pool control.

(B) Transwell migration assay post knockdown/inhibition of c-MET or EphA2 or both and HGF as a chemotactic factor on MDA-MB-231 cells.

(C) Transwell invasion assay post knockdown/inhibition of EphA2 and c-MET or both and HGF as a chemotactic factor on MDA-MB-231 cells.

(D) A schematic representation of the mammosphere formation assay.

(E) Mammosphere formation assay post knockdown/inhibition of c-MET or EphA2 or both in the presence of HGF.

(F) Matrigel tube formation assay post knockdown/inhibition of c-MET or EphA2 or both in the presence of HGF.

(G) Representative photomicrograph of freshly harvested breast tumors with a ruler (below) for scale.

(H) Graph representing the tumor volume vs. the various groups. Data are representative of triplicate experiments (mean ± SD). *$p < 0.05$ statistically significant difference compared to corresponding control by one-way ANOVA. Scale bars: 100 μm. Also see, Figures S3 and S4.

Lupeol and 5FU combined treatment imparts synergistic cytotoxic effect and abrogates wound healing

To evaluate the cytotoxic effects of the combined treatment of 5FU and Lupeol on TNBC in an *in vitro* setting, the IC50 of Lupeol and 5FU was determined by performing the MTT cell viability assay of MDA-MB-231 cells. The cell viability graph depicting the percent cell viability

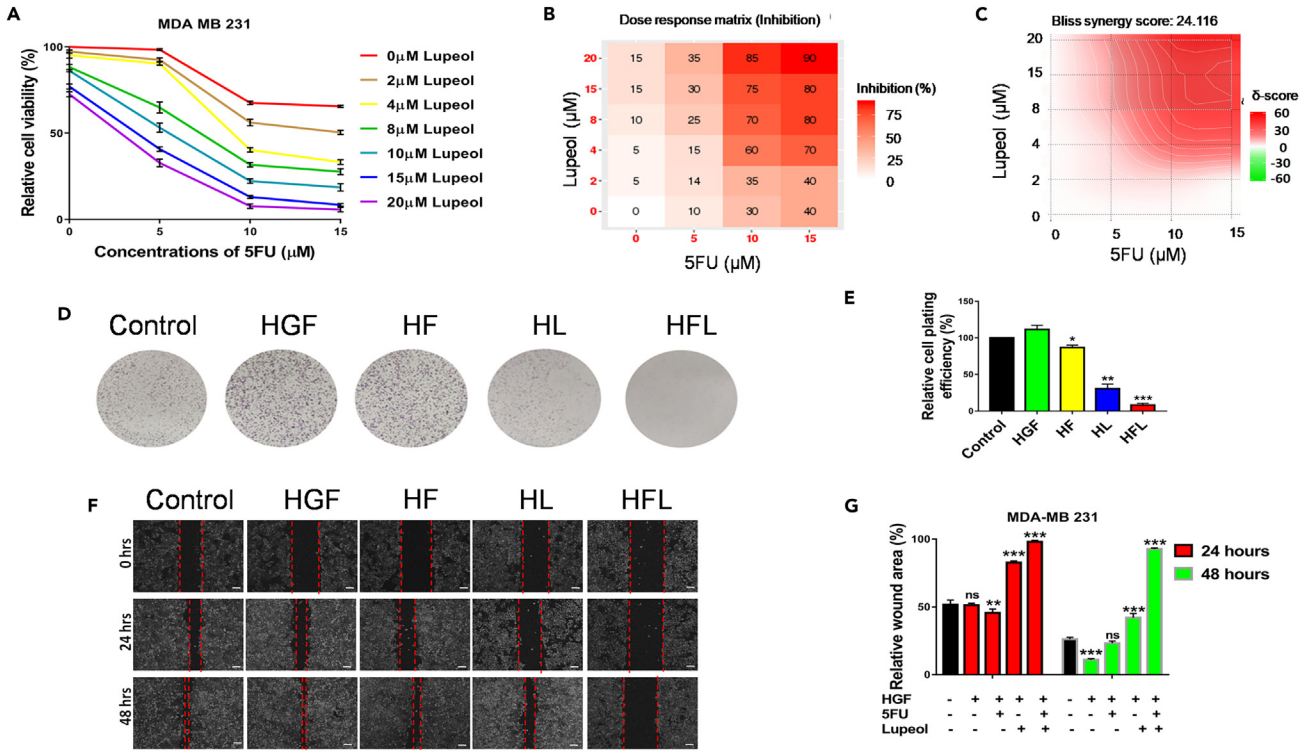

Figure 3. Combination of Lupeol and 5FU induces cytotoxicity on MDA-MB-231 cells and also reduce their wound healing potential

(A) Percentage cell viability graph depicting the various Combination treatment of MDA-MB-231 cells with Lupeol (0–20 μM) and 5FU (0, 5, 10, and 15 μM).

(B) Dose response heatmap based on percentage inhibition of cell viability following combination of Lupeol (0–20 μM) and 5FU (0–15 μM) in MDA-MB-231 cells. Scale represents the spectrum where increase in the intensity of red color indicates higher percentage of inhibition.

(C) The synergy distribution map of the combination of Lupeol and 5FU using Bliss synergy model that calculated Bliss synergy score.

(D) Colony formation assay post treatment with Lupeol (8 μM) and/or 5FU (10 μM) of MDA-MB-231 cells (in the presence of HGF).

(E) Graph representing the relative cell plating efficiency (%) of MDA-MB-231.

(F) Wound healing assay post treatment with Lupeol (8 μM) and/or 5FU (10 μM) on MDA-MB-231 cells in the presence of HGF (100 ng/mL) for 24 and 48 h.

(G) Graph representing the relative wound area (%) over 24 and 48 h. Data are representative of triplicate experiments (mean ± SD). *p < 0.05 and ***p < 0.001 statistically significant difference compared to corresponding control by one-way ANOVA. ns = not significant; HGF = hepatocyte growth factor; HF = HGF+5FU; HL = HGF+Lupeol; HFL = HGF+5FU + Lupeol. Scale bars: 500 μm. Also see, Table S7.

and a dose response matrix were presented as heatmap for drug induced inhibition of viability using MDA-MB-231 cells (Figures 3A and 3B respectively) while treated with various doses of Lupeol and 5FU are shown. The IC50 concentration of Lupeol was 8.651 μM and 5FU was 10 μM. The SynergyFinder 3.0 tool revealed a Bliss synergy score of 24.116 (mean) and presented as a synergy distribution map depicted in Figure 3C. The combination Index (CI) for MDA-MB-231 was calculated to be 0.562 (Table S7). The CI is less than 0.9, proving that the combination regimen is synergistic in nature. Notably, the dose reduction index (DRI) for 5FU while in combination with Lupeol was observed to be 3.71 for MDA MB 231 cells. From the colony formation assay, it is evident that the combination of Lupeol and 5FU is the most effective in reducing the cell plating efficiency and thus colony formation potential MDA-MB-231 (even in the presence of HGF) (Figures 3D and 3E). Also, the wound healing assay revealed that the combination of Lupeol and 5FU was the most efficient in diminishing the wound healing potential of the MDA-MB-231 cells (Figures 3F and 3G) than the individual compounds even in the presence of HGF, over a period of 48 h.

Combination of Lupeol and 5FU induces apoptosis of breast cancer cells *in vitro*

In order to evaluate the potential to induce apoptosis in TNBC cells, the Annexin V/PI apoptosis assay was performed in MDA-MB-231 (Figures 4A and 4B) cells. Notably, the combination arm induced apoptosis in the cell line compared to the individually treated arms, in the presence of HGF challenge in milieu. The subsequent expression of the pro-apoptotic protein Bax was evaluated by immunofluorescence staining (Figures 4C and 4D). The combination arm showed the most corrected total cell fluorescence (CTCF) indicating the maximum expression of Bax. Western blot analysis confirmed this elevated expression of Bax in the combination arm in the MDA-MB-231 cells (Figures 4E and 4F). Concomitantly, the expression of the anti-apoptotic protein Bcl2 decreased significantly and was found to be least expressed in the combination arm (Figures 4E and 4G).

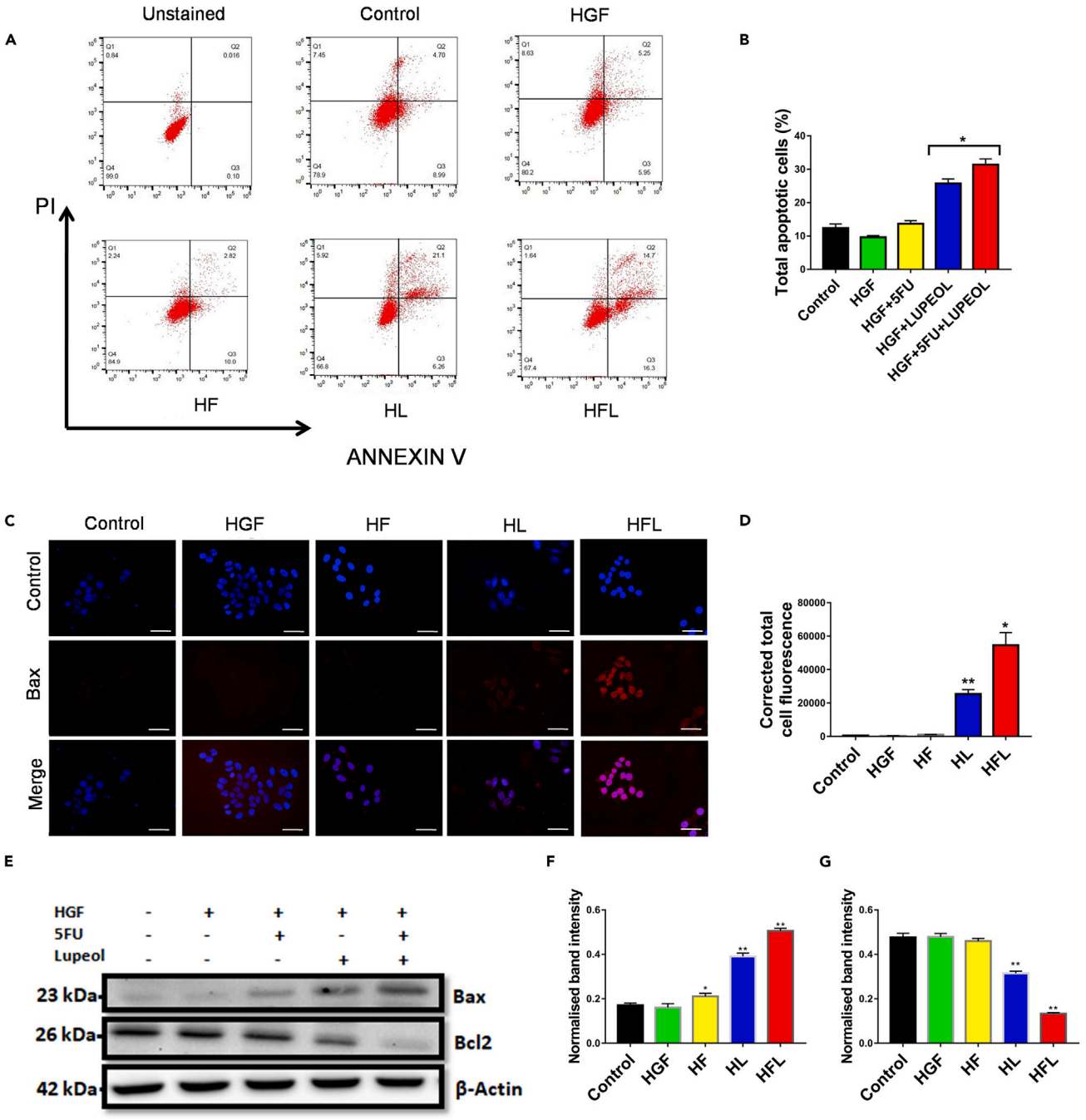

Figure 4. Induction of apoptosis by the combination regimen of Lupeol and 5FU on MDA-MB-231 cells

(A) Annexin V/PI apoptosis assay by flow cytometry post treatment with Lupeol or 5FU or both on MDA-MB-231 cells (in the presence of HGF).

(B) Graph representing the total apoptotic cells (%) for various treatment arms of MDA-MB-231.

(C) Immunofluorescence staining to detect Bax protein (exhibiting red fluorescence) post treatment with Lupeol and 5FU or both on MDA-MB-231 cells (in the presence of HGF).

(D) Graph representing the corrected total cell fluorescence (CTCF) of various treatment arms of MDA-MB-231 cells.

(E) Western blot analysis probed for Bax and Bcl2 proteins post treatment with Lupeol or 5FU or both on MDA-MB-231 cells (in the presence of HGF).

(F) Graph representing the normalized band intensity of Bax protein of various treatment arms of MDA-MB-231 cells.

(G) Graph representing the normalized band intensity of Bcl2 protein of various treatment arms of MDA-MB-231 cells. Data are representative of triplicate experiments (mean ± SD). *$p < 0.05$ and ***$p < 0.001$ statistically significant difference compared to corresponding control by one-way ANOVA. HGF = hepatocyte growth factor; HF = HGF+5FU; HL = HGF+Lupeol; HFL = HGF+5FU + Lupeol. Scale bars: 100 μm.

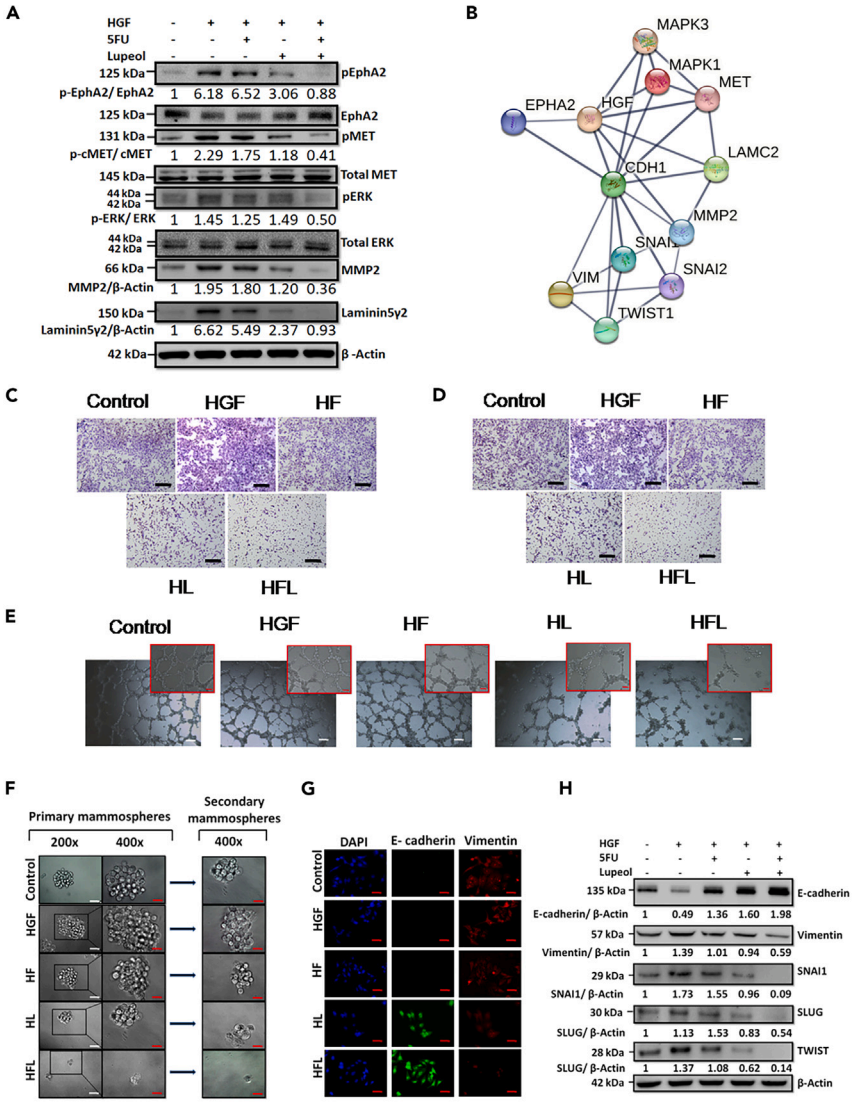

Figure 5. Evaluation of the combinatorial effect of Lupeol and 5FU on MDA-MB 231 cells

(A) Western blot analysis of MDA-MB-231 cells treated with 5FU, Lupeol, or both in the presence of HGF and probed for phospho-EphA2 (S897), EphA2, phospho-c-MET, total c-MET, pERK1/2, total ERK1/2, MMP2 and Laminin-5Y2 protein expression. β- Actin was used as a loading control.

(B) Protein-protein interaction (PPI) network analysis using input proteins from the present study using STRING platform showing interacting molecules and edge confidence levels in the network.

(C and D) Transwell migration and invasion of MDA-MB-231 cells upon treatment with Lupeol, 5FU or both, while HGF was used as a chemotactic factor (Scale bars: 100 μm).

(E) Matrigel tube formation of MDA-MB-231 cells upon treatment with Lupeol, 5FU, or both in the presence of HGF (Scale bars: 500 μm and 100 μm in inset).

(F) Primary and secondary Mammosphere formation of MDA-MB-231 cells in the presence of HGF and treated with 5FU, Lupeol, or both (Scale 200 μm in white and 100 μm in red).

(G) Immunofluorescence staining of MDA-MB-231 cells for the detection of E-cadherin (green) and Vimentin (red) post treatment with Lupeol or 5FU or both in the presence of HGF (Scale bars: 100 μm).

(H) Western blot analysis of MDA-MB-231 cells treated with Lupeol, 5FU, or both in the presence of HGF and probed for E-cadherin, Vimentin, SNAI1, SLUG, and TWIST. Data are representative of triplicate experiments (mean ± SD). HGF = hepatocyte growth factor; HF = HGF+5FU; HL = HGF+Lupeol; HFL = HGF+5FU + Lupeol. Also see, Figure S5.

Lupeol and 5FU treatments synergize to impart cytotoxic effect and also induce reversal of EMT on MDA-MB- 231 cells

Upon evaluation of the modulation of critical proteins, it was observed that the combination arm was most efficacious in significantly down-regulating the phosphorylation of both c-MET and EphA2 and the downstream molecules (Figure 5A). *In silco* protein-protein interaction (PPI) network simulation revealed significant interactions with several molecules involved in the modulation of epithelial mesenchymal transition

(EMT) (Figure 5B). MDA-MB-231 cells, representing the TNBC subtype, display a mesenchymal phenotype with high migratory and invasive potential. HGF further enhanced the mesenchymal characteristics. However, subsequent treatment with Lupeol and 5FU in combination reduced the migratory and invasive potential of MDA-MB-231 cells when HGF acted as a chemotactic factor, as is evident from the transwell migration and invasion assays (Figures 5C and 5D). To delineate the impact of Lupeol and 5FU in the context of invasive properties, we profiled vasculogenic mimicry using the Matrigel tube formation assay in MDA-MB-231 cells *in vitro* upon subsequent treatment with HGF, Lupeol, and 5FU alone or in combination (Figure 5E). The combination group showed tubes with the least number of intercellular junctions and minimum vessel length among all groups. In parallel, upon treatment with HGF, MDA-MB-231 cells tended to form increased numbers of mammospheres with significantly larger diameters, when compared to the control arm. Subsequent treatment with Lupeol and 5FU alone or in combination most significantly abrogated the mammosphere-forming capability of the cells. Notably, this effect was sustained even in the secondary mammosphere-forming potential of the MDA-MB-231 cells originating from the treatment arms, even when the treatment stress was relieved (Figure 5F; Figures S5A and S5B). Dual immune-fluorescence staining of MDA-MB-231 cells for epithelial marker E-cadherin and mesenchymal marker vimentin revealed that the combination regimen of Lupeol and 5FU resulted in a reversal of EMT (Figure 5G). The maximum expression of E-cadherin and minimum expression of vimentin were observed in the combined treatment group Figure 5H; Figures S5C and S5D. Subsequently, the differential expression of critical markers implicated in the induction of EMT, such as SNAI1, SLUG, and TWIST, was also evaluated by western blotting, which further confirmed the significantly diminished expression of these positive EMT regulators in the combination arm compared to the individually treated arms (Figure 5H).

Systemic evaluation of the combinatorial effect of 5FU and Lupeol

$4T1^{luc2}$ TNBC cells derived from BALB/c mice were used to induce syngeneic TNBC tumors in female BALB/c mice. After tumor induction (5 days after the injection of $4T1^{luc2}$ cells into abdominal mammary fat pads), when the tumor reached a dimension of 5 × 5 mm, the mice were treated with 5FU and/or Lupeol along with HGF (Figure 6A). In this live animal model, tumor growth was monitored by *in vivo* animal imaging using IVIS, which detects bioluminescence as a measure of viable tumor cell density (Figure 6B). Prior to this *in vivo* dosing schedule, a separate group of non-tumor-bearing mice was administered the same treatment regimens to check for impending off-target toxicity. No significant alterations were observed in the major organs (pathology) or biochemical parameters in the blood of the exposed mice (Figure S6; Table S8). It was observed that there was a significant inhibition of tumor growth in the combination arm, even in the presence of HGF, compared to the other groups (Figures 6C–6E). IHC staining of the harvested tumors revealed a marked reduction in the expression of Ki-67 and an increase in Caspase 3c expression (Figure 6F). Notably, the phosphorylation of EphA2, c-MET, and their downstream molecules was significantly reduced in the combination arm, thus confirming the efficacy of the combination regimen (Figure 6G).

Perturbation of the c-MET and EphA2 activation upon combined exposure to 5FU and Lupeol in patient tumor derived *ex vivo* model

To demonstrate the mechanistic regulation of c-MET and EphA2 signaling axes by Lupeol and 5FU, an *ex vivo* explant culture was performed in freshly acquired breast cancer tissues (N = 10), and their nodal status (N) and tumor stage (T) are shown in Figure 7A. Upon probing the tissue sections for Ki67 and Caspase 3c (Figure 7B), we observed that the expression of Ki67 in the combination arm was significantly reduced (Figure 5C). Concomitant induction of Caspase 3c was also observed (Figure 7D). IHC profiling of serial tissue sections for the activation status of c-MET and EphA2 (Figure 7E) revealed that the phosphorylation of EphA2 (Figure 7F) and c-MET (Figure 7G) was significantly abrogated in the combination-treated group. Subsequently, the induction of apoptosis on human TNBC tumors (N = 7) (Table S9) was evaluated by exposing them to various standards of care and also the 5FU and Lupeol combination (Figure 7H). It revealed that the combination of 5FU and Lupeol had comparable, sometimes even better induction of apoptosis than the other SOCs.

DISCUSSION

ER-negative, PR-negative, HER2 negative breast cancer, commonly known as TNBC,[34] is one of the most challenging breast cancer molecular subtypes, and achieving durable therapeutic success using current treatment paradigms is far from our expectations. Due to its special phenotypic status, TNBC does not respond to molecular-targeted therapy, even to endocrine therapy. Therefore, chemotherapy is the only systemic treatment option. Unfortunately, the prognosis of TNBC patients undergoing conventional postoperative adjuvant chemo-radiotherapy is poor. Tumor recurrence and metastatic progression eventually occur due to residual lesions that persist and often disseminate as drug-tolerant cells.[35,36] One of the potential drivers of this frequent treatment failure is the perturbation of multiple oncogenic RTK signaling axes. Aberrant c-Met signaling has been reported in various cancer types and is regarded as a novel therapeutic target.[37] High levels of c-MET and its phosphorylated form have been observed in all breast cancer subtypes, and are correlated with poor prognosis.[38] The similar mechanistic underpinnings of EphA2 lend credence to this pathway as a promising therapeutic (druggable) target for breast cancer because its deactivation/downregulation can be actionable and therefore inhibited by multiple regimens for restoring sensitivity to drugs.[17] Here, we evaluated the underlying downstream molecular mechanism and subsequent phenotypic modulation of TNBC in the presence of HGF in a model system in which c-MET, EphA2, or both were silenced. The following two strategies were implemented: (1) silencing with specific siRNAs and, (2) specific inhibitors of receptor phosphorylation. Both strategies yielded similar results. Treating known TNBC cell lines, such as MDA-MB-231, with HGF increased the phosphorylation of both EphA2 and c-MET receptors. This prospectively resulted in the increased phosphorylation of ERK 1/2 which cascaded to the increased expression of potent extracellular matrix remodeling factors like MMP-2 and ultimately Laminin-5γ2.

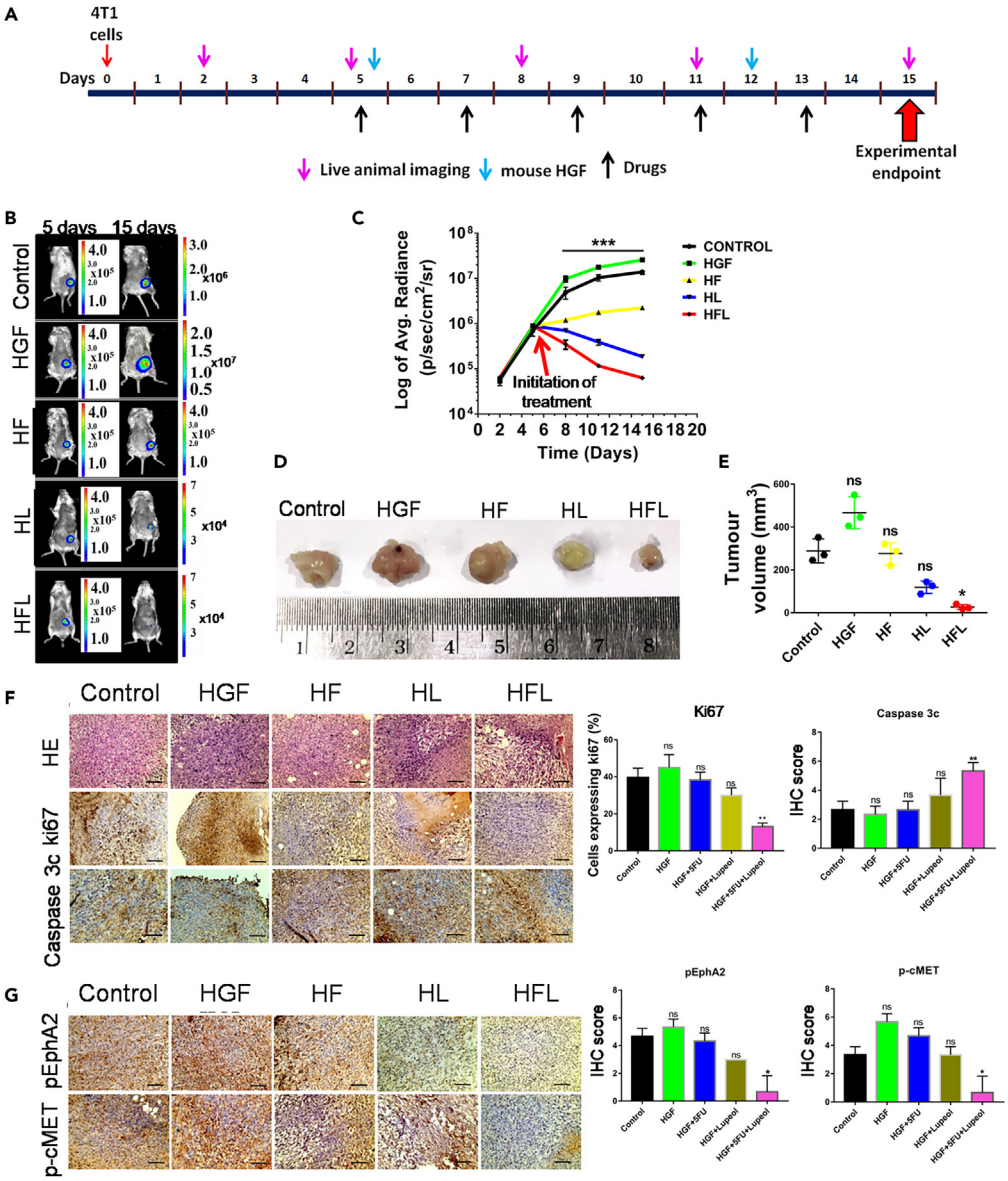

Figure 6. *In vivo* evaluation of the combinatorial effect of Lupeol and 5FU in a TNBC syngeneic mice model

(A) Schematic representation of dosing schedule (all compounds were administered intraperitoneally).

(B) *In vivo* live animal images of the 4T1^{luc2} induced tumors in various treatment arms in BALB/c mice at day 5 (initiation of treatment) and at day 15 (experimentation endpoint).

(C) Graph representing the log of average radiance vs. Time of the tumor growth.

(D) Representative photomicrograph of freshly harvested breast tumors with a ruler (below) for scale.

(E) Graph representing the tumor volume vs. the various treatment arms.

(F) Representative images of Hematoxylin and Eosin stain followed by IHC staining for Ki67 and Caspase 3c in the sections of harvested tumors developed in BALB/c mice along with their quantitative graphs.

(G) Representative images of the IHC staining to evaluate the differential expression of phospho-EphA2 and phospho-cMET in the tumors of the various treatment arms along with their quantitative graphs. *$p < 0.05$ and ***$p < 0.001$ statistically significant difference compared to corresponding control by one-way ANOVA. Data are representative of triplicate experiments (mean ± SD) ns = not significant; HGF = hepatocyte growth factor; HF = HGF+5FU; HL = HGF+Lupeol; HFL = HGF+5FU + Lupeol. Scale bars: 200 μm. Also see, Figure S6 and Table S8.

Notably, the individual knockdown of these receptors diminished the expression of these effector molecules. Indeed, some cells were able to evade this strategy and successfully retain their migratory and invasive potential. Single knockdown also failed to prevent TNBC cells from forming mammospheres or tubes in the presence of Matrigel. This observation indicates that single-target knockdown or pharmacological

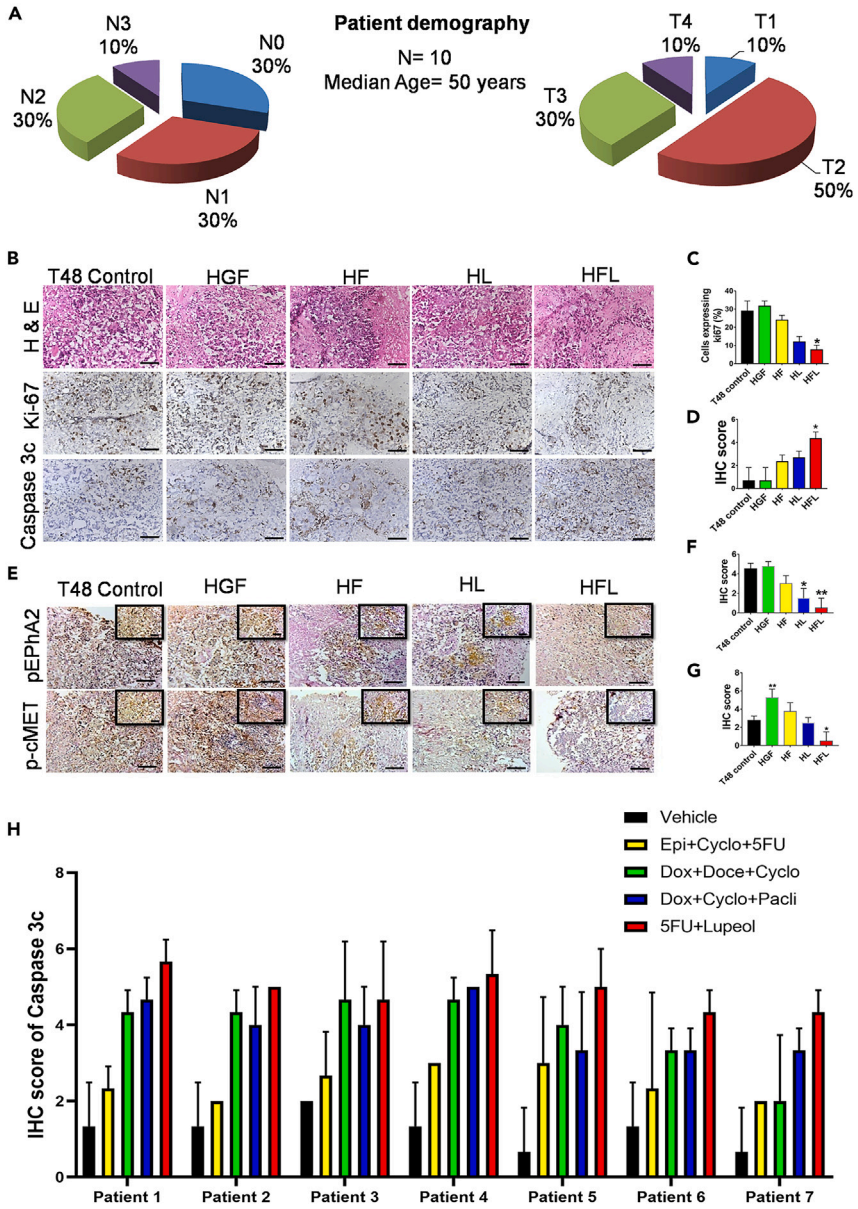

Figure 7. Evaluation of the combinatorial effect of 5FU and Lupeol in *ex vivo* explant culture model

(A) Graphical representation of the patient data used in this experiment, pertaining to the nodal status and tumor stage.

(B) Representative images of IHC staining of TNBC tissue fragments, post exposure to HGF, 5FU, Lupeol alone or in combination cells for the detection of Ki67 and Caspase 3c protein expression (Scale bars: 200 μm).

(C) Graph representing the percentage of cells expressing Ki67 vs. the various treatment arms.

(D) Graph representing the IHC score of Caspase 3c vs. various treatment arms.

(E) Representative images of IHC staining for the evaluation of phospho-EphA2 and phospho-cMET in various treatment arms (Scale bars: 200 μm and 100 μm in inset).

(F) Graph representing the various IHC scores of phospho-EphA2 in various treatment arms.

(G) Graph representing the various IHC scores of phospho-cMET in various treatment arms.

(H) Graph representing the various IHC scores of Caspase 3c expression in TNBC tumors (N = 7) after treating them with various SOC and 5FU and Lupeol combination. Data are representative of triplicate experiments (mean ± SD). *$p < 0.05$ statistically significant difference compared to corresponding control by one-way ANOVA. HGF = hepatocyte growth factor; HF = HGF+5FU; HL = HGF+Lupeol; HFL = HGF+5FU + Lupeol. Also see, Table S9.

inhibition might decrease the aggressiveness of the cells but fail to abrogate their various characteristics completely as one of the signaling axes compensates for the other in a context when one remains largely unperturbed. This prompted us to adopt a dual knockdown/inhibition strategy, which was more effective in downregulating the expression of effector molecules even in the presence of HGF. In addition, the migratory, invasive, mammosphere formation, and Matrigel tube formation potential of MDA-MB-231cells were successfully inhibited by this dual knockdown/inhibition strategy. We further validated these findings using a TNBC syngeneic mouse model. Consistent with our *in vitro* findings, the *in vivo* tumorigenic potential of 4T1 cells was most significantly abrogated in the dual-silenced group.

Chemotherapy remains the mainstay of treatment for TNBC and 5FU is one of a critical agent in the NCCN-approved regimen. However, in addition to the limited response rate, between 31% and 34% of individuals receiving 5FU exhibit dose-limiting toxicities.[39] Fluoronucleotide incorporation into RNA and DNA, as well as the direct inhibition of thymidylate synthase, has been identified as the main mechanisms of cytotoxicity caused by 5FU.[40] Hematological and gastrointestinal adverse effects are more frequent in patients receiving 5FU.[41] A recent study also devalues the use of 5FU in high-risk early breast cancer and recommends its exclusion from therapeutic regimens citing its worsening toxicity and lack of long term effects when included in the chemotherapeutic regimens.[42] As monotherapy generally does not maximize chemo-drug efficacy, 5FU is co-administered with other substances to boost its effectiveness.[43] Lupeol is a natural phytochemical that has shown cytotoxic effects on cancer cells and is highly effective in inducing apoptosis.[21,22] Also, the strategy of metronomic chemotherapy which has potential to make promising impact in breast cancer treatment[44] paves the way for investigating the therapeutic cooperation of these two drugs in our study which may help in reducing the burden of 5FU dose that are effective at clinics. The synergistic effect of the combinatorial strategy of Lupeol and 5FU that we adopted was tested on a TNBC cell line MDA-MB-231 and proved to be effective in reducing the proliferation and wound healing potential. In addition, MDA-MB-231 cells are phenotypically mesenchymal, and thus notorious owing to their multidrug resistance.[45,46] As MDA-MB-231 cells contextually preserve a mesenchymal phenotype, we evaluated the effect of the combination regimen on these cells. There was a marked change in the migratory and invasive potentials of the cells. This can be attributed to a mechanistic shift in which the mesenchymal characteristics of the cells decrease and the epithelial characteristics become more pronounced. In other words, the combination of 5FU and Lupeol orchestrated the EMT reversal. To substantiate this response, we selectively profiled the expression of mesenchymal markers (Vimentin, TWIST, SNAI1, and SLUG) and observed augmented expression when cells were exposed to HGF. However, upon subsequent treatment, expression was significantly reduced in the combination arm. In contrast, the combination resulted in increased expression of E-cadherin, despite the active engagement of HGF in the milieu. Furthermore, the data obtained from the cell line require further validation using more complex and clinically relevant systems to ascertain a better translational impact. To bridge this gap, we used an *in vivo* syngeneic mouse model and an *ex vivo* patient tumor-derived live tumor slice culture model that maintains the key phenotypes and heterogeneity of the original patient tumor microenvironment in short-term culture and therefore provides a suitable context for delineating the mechanistic underpinnings of signaling crosstalk and reliably modeling drug effects. Prior studies have evidences regarding the bio-availability of Lupeol in the serum of animals used for experimentation which makes Lupeol a suitable candidate for testing combination therapies.[34,47–49] Indeed, both of these models confirmed that the combination regimen reduced the proliferative potential of breast cancer cells and induced apoptosis in a ligand (HGF)-complemented niche.

Endothelia-independent networks are associated with highly aggressive metastatic tumors and poor patient survival.[50–52] In our earlier study, we elucidated site-specific phosphorylation of the EphA2 receptor in conjunction with vasculogenic mimicry as an indicator of poor prognosis in breast cancer patients.[19] We observed that in the presence of HGF, the MDA-MB-231 cell line phenocopying TNBC formed more robust tubes in Matrigel. Notably, these tubes were disrupted or failed to assume a mature architecture upon subjecting them to the combination of Lupeol and 5FU. Subsequently, it was revealed that the combination regimen significantly downregulated both c-MET and EphA2 signaling axes, as well as their downstream effector molecules. We hypothesize that this receptor inhibition of Lupeol might be the cause of its anti-cancer effect and paves the way for more elaborate studies to leverage its role as a novel anticancer therapeutic.

To the best of our knowledge, this is the first study to elucidate the effect of a combination regimen consisting of Lupeol and 5FU in breast cancer *in vitro, in vivo*, and *ex vivo* models. Taken together, our results suggest that this combination has the capacity to comprehensively inhibit the diverse phenotypic modalities of breast cancer cells, especially the clinically elusive TNBC subtype. We did not observe any clinical signs or symptoms of toxicity in the combinational group of mice. However, further toxicity studies are required in larger animals prior to clinical studies. Our data suggest that this combination can prevent tumor recurrence, increase survival, and enhance the quality of life of patients with TNBC.

Limitations of the study

In the present study, we largely relied on syngeneic mice model for elucidating synergy effects which could have been further substantiated in patient-derived xenograft models. Furthermore, even though Lupeol demonstrated good safety profile in animal model and conform synergy in *in vitro*, *in vivo* and *ex vivo*, all three key experimental platforms, the lack of putative evidence of binding is one key limitation for understanding its direct or indirect interaction with the potential molecular targets. Delineation of *ex vivo* TNBC phenotypes and anti TNBC effects of Lupeol and 5FU in our present study are based on a small size of patient samples as availability of actionable TNBC sample is a major rate limiting step. Therefore, it is obvious that further validation on a larger cohort will lend translational credence to our study hypothesis and extend the therapeutic opportunities.

ETHICAL APPROVAL

This study was approved by the Institutional Ethics Committee and Institutional Animal Ethics Committee at the Chittaranjan National Cancer Institute, Kolkata (IEC Ref: A-4.311/NM/26/11/2018) and IAEC-1774/NM-18/2021/17. All procedures performed in this study involving human

participants were in accordance with the ethical standards of the institutional and/or national research committee and with the1964 Helsinki Declaration and its later amendments or comparable ethical standards.

STAR★METHODS

Detailed methods are provided in the online version of this paper and include the following:

- KEY RESOURCES TABLE
- RESOURCE AVAILABILITY
  - Lead contact
  - Materials availability
  - Data and code availability
- EXPERIMENTAL MODEL AND STUDY PARTICIPANT DETAILS
  - Patients and samples
  - Cell lines and reagents
  - Mice
- METHOD DETAILS
  - Patient cohort stratification and follow-up
  - *Ex vivo* tumor fragment culture
  - Immunohistochemistry staining
  - siRNA mediated silencing
  - Pharmacological regulation
  - Western blotting
  - Transwell invasion and migration
  - Mammosphere formation assay
  - Tube formation assay
  - *In vivo* experiments
  - Cytotoxicity assay
  - Determination of combination effect
  - Colony formation assay
  - Wound healing assay
  - Apoptosis assay
  - Immunofluorescence staining
  - Protein-protein interaction (PPI) analysis and network modeling
- QUANTIFICATION AND STATISTICAL ANALYSIS

SUPPLEMENTAL INFORMATION

Supplemental information can be found online at https://doi.org/10.1016/j.isci.2023.108395.

ACKNOWLEDGMENTS

We acknowledge the immense support provided by Dr. Jayanta Chakrabarti, Director, Chittaranjan National Cancer Institute, Kolkata, throughout the project. Authors also acknowledge the suggestions provided by Dr. Sayantan Bhattacharyya, UT MD Anderson Cancer Center, USA in preparing the graphical abstract. The graphical abstract was created with BioRender.com. The structure of 5-fluorouracil (CID: 3385) and Lupeol (CID: 259846) in the graphical abstract was obtained from PubChem (https://pubchem.ncbi.nlm.nih.gov/). This study was supported by Chittaranjan National Cancer Institute, Kolkata, India.

AUTHOR CONTRIBUTIONS

D.M. and N.M. conceptualized and designed the study. D.M. and D.S. performed the experiments. D.M., R.M., G.D., and S.B. analyzed the data. D.M., G.D., A.M., and N.M. interpreted the data. N.A. and P.N. contributed to providing tissue specimens and clinical insights. S.M.M. provided histopathological insights. A.M., B.M., and N.M. provided valuable insights into the manuscript. D.M. drafted the manuscript. B.M., A.M., and N.M. reviewed and edited the manuscript. D.M., A.M., B.M., and N.M. revised the manuscript. All authors approved the submitted version of the manuscript.

DECLARATION OF INTERESTS

Authors have no conflict of interest to declare.

Received: August 7, 2023
Revised: October 2, 2023
Accepted: November 2, 2023
Published: November 4, 2023

REFERENCES

1. Sung, H., Ferlay, J., Siegel, R.L., Laversanne, M., Soerjomataram, I., Jemal, A., and Bray, F. (2021). Global Cancer Statistics 2020: GLOBOCAN Estimates of Incidence and Mortality Worldwide for 36 Cancers in 185 Countries. CA. Cancer J. Clin. *71*, 209–249. https://doi.org/10.3322/caac.21660.
2. Cerrito, M.G., De Giorgi, M., Pelizzoni, D., Bonomo, S.M., Digiacomo, N., Scagliotti, A., Bugarin, C., Gaipa, G., Grassilli, E., Lavitrano, M., et al. (2018). Metronomic combination of Vinorelbine and 5Fluorouracil is able to inhibit triple-negative breast cancer cells. Results from the proof-of-concept VICTOR-0 study. Oncotarget *9*, 27448–27459. https://doi.org/10.18632/oncotarget.25422.
3. Yin, L., Duan, J.-J., Bian, X.-W., and Yu, S.C. (2020). Triple-negative breast cancer molecular subtyping and treatment progress. Breast Cancer Res. *22*, 61. https://doi.org/10.1186/s13058-020-01296-5.
4. Shapiro, C.L., and Recht, A. (2001). Side Effects of Adjuvant Treatment of Breast Cancer. N. Engl. J. Med. *344*, 1997–2008. https://doi.org/10.1056/NEJM200106283442607.
5. (2017). Rationalizing combination therapies. Nat. Med. *23*, 1113. https://doi.org/10.1038/nm.4426.
6. Wilson, M.A., Zhao, F., Khare, S., Roszik, J., Woodman, S.E., D'Andrea, K., Wubbenhorst, B., Rimm, D.L., Kirkwood, J.M., Kluger, H.M., et al. (2016). Copy Number Changes Are Associated with Response to Treatment with Carboplatin, Paclitaxel, and Sorafenib in Melanoma. Clin. Cancer Res. *22*, 374–382. https://doi.org/10.1158/1078-0432.CCR-15-1162.
7. Gaule, P.B., Crown, J., O'Donovan, N., and Duffy, M.J. (2014). cMET in triple-negative breast cancer: is it a therapeutic target for this subset of breast cancer patients? Expert Opin. Ther. Targets *18*, 999–1009. https://doi.org/10.1517/14728222.2014.938050.
8. Okuyama, T., Sakamoto, R., Kumagai, K., Nishizawa, M., Kimura, T., Sugie, T., and Kimura, T. (2020). EPHA2 antisense RNA modulates EPHA2 mRNA levels in basal-like/triple-negative breast cancer cells. Biochimie *179*, 169–180. https://doi.org/10.1016/j.biochi.2020.10.002.
9. Nikas, I., Giaginis, C., Petrouska, K., Alexandrou, P., Michail, A., Sarantis, P., Tsourouflis, G., Danas, E., Pergaris, A., Politis, P.K., et al. (2022). EPHA2, EPHA4, and EPHA7 Expression in Triple-Negative Breast Cancer. Diagnostics *12*, 366. https://doi.org/10.3390/diagnostics12020366.
10. Zhao, X., Qu, J., Hui, Y., Zhang, H., Sun, Y., Liu, X., Zhao, X., Zhao, Z., Yang, Q., Wang, F., and Zhang, S. (2017). Clinicopathological and prognostic significance of c-Met overexpression in breast cancer. Oncotarget *8*, 56758–56767. https://doi.org/10.18632/oncotarget.18142.
11. Chaudhary, S.S., Choudhary, S., Rawat, S., Ahir, G., Bilgrami, A.L., and Ashraf, G.M. (2020). c-Met as a potential therapeutic target in triple negative breast cancer. Cancer Lead. Proteases, 295–326. https://doi.org/10.1016/B978-0-12-818168-3.00011-5.
12. Albiges, L., Heng, D.Y.C., Lee, J.L., Walker, S., Mellemgaard, A., Ottesen, L., Frigault, M.M., L'Hernault, A., Wessen, J., Choueiri, T., et al. (2022). Impact of MET status on treatment outcomes in papillary renal cell carcinoma: A pooled analysis of historical data. Eur. J. Cancer *170*, 158–168. https://doi.org/10.1016/j.ejca.2022.04.021.
13. Organ, S.L., and Tsao, M.-S. (2011). An overview of the c-MET signaling pathway. Ther. Adv. Med. Oncol. *3*, S7–S19. https://doi.org/10.1177/1758834011422556.
14. Straussman, R., Morikawa, T., Shee, K., Barzily-Rokni, M., Qian, Z.R., Du, J., Davis, A., Mongare, M.M., Gould, J., Frederick, D.T., et al. (2012). Tumour micro-environment elicits innate resistance to RAF inhibitors through HGF secretion. Nature *487*, 500–504. https://doi.org/10.1038/nature11183.
15. Wang, M., Zhao, J., Zhang, L., Wei, F., Lian, Y., Wu, Y., Gong, Z., Zhang, S., Zhou, J., Cao, K., et al. (2017). Role of tumor microenvironment in tumorigenesis. J. Cancer *8*, 761–773. https://doi.org/10.7150/jca.17648.
16. Liebmann, C. (2001). Regulation of MAP kinase activity by peptide receptor signalling pathway: paradigms of multiplicity. Cell. Signal. *13*, 777–785. https://doi.org/10.1016/s0898-6568(01)00192-9.
17. Zhao, P., Jiang, D., Huang, Y., and Chen, C. (2021). EphA2: A promising therapeutic target in breast cancer. J. Genet. Genom. *48*, 261–267. https://doi.org/10.1016/j.jgg.2021.02.011.
18. Harada, K., Negishi, M., and Katoh, H. (2015). HGF-induced serine 897 phosphorylation of EphA2 regulates epithelial morphogenesis of MDCK cells in 3D culture. J. Cell Sci. *128*, 1912–1921. https://doi.org/10.1242/jcs.163790.
19. Mitra, D., Bhattacharyya, S., Alam, N., Sen, S., Mitra, S., Mandal, S., Vignesh, S., Majumder, B., and Murmu, N. (2020). Phosphorylation of EphA2 receptor and vasculogenic mimicry is an indicator of poor prognosis in invasive carcinoma of the breast. Breast Cancer Res. Treat. *179*, 359–370. https://doi.org/10.1007/s10549-019-05482-8.
20. Sharma, N., Palia, P., Chaudhary, A., Verma, K., and Kumar, I. (2020). A Review on Pharmacological Activities of Lupeol and its Triterpene Derivatives. J. Drug Delivery Ther. *10*, 325–332. https://doi.org/10.22270/jddt.v10i5.4280.
21. Bhattacharyya, S., Sekar, V., Majumder, B., Mehrotra, D.G., Banerjee, S., Bhowmick, A.K., Alam, N., Mandal, G.K., Biswas, J., Majumder, P.K., and Murmu, N. (2017). CDKN2A-p53 mediated antitumor effect of Lupeol in head and neck cancer. Cell. Oncol. *40*, 145–155. https://doi.org/10.1007/s13402-016-0311-7.
22. Rauth, S., Ray, S., Bhattacharyya, S., Mehrotra, D.G., Alam, N., Mondal, G., Nath, P., Roy, A., Biswas, J., and Murmu, N. (2016). Lupeol evokes anticancer effects in oral squamous cell carcinoma by inhibiting oncogenic EGFR pathway. Mol. Cell. Biochem. *417*, 97–110. https://doi.org/10.1007/s11010-016-2717-y.
23. Bhattacharyya, S., Mitra, D., Ray, S., Biswas, N., Banerjee, S., Majumder, B., Mustafi, S.M., and Murmu, N. (2019). Reversing effect of Lupeol on vasculogenic mimicry in murine melanoma progression. Microvasc. Res. *121*, 52–62. https://doi.org/10.1016/j.mvr.2018.10.008.
24. Liu, K., Zhang, X., Xie, L., Deng, M., Chen, H., Song, J., Long, J., Li, X., and Luo, J. (2021). Lupeol and its derivatives as anticancer and anti-inflammatory agents: Molecular mechanisms and therapeutic efficacy. Pharmacol. Res. *164*, 105373. https://doi.org/10.1016/j.phrs.2020.105373.
25. Che, S., Wu, S., and Yu, P. (2022). Lupeol induces autophagy and apoptosis with reduced cancer stem-like properties in retinoblastoma via phosphoinositide 3-kinase/protein kinase B/mammalian target of rapamycin inhibition. J. Pharm. Pharmacol. *74*, 208–215. https://doi.org/10.1093/jpp/rgab060.
26. Malekinejad, F., Kheradmand, F., Khadem-Ansari, M.H., and Malekinejad, H. (2022). Lupeol synergizes with doxorubicin to induce anti-proliferative and apoptotic effects on breast cancer cells. Daru *30*, 103–115. https://doi.org/10.1007/s40199-022-00436-w.
27. Wilson, K., Shiuan, E., and Brantley-Sieders, D.M. (2021). Oncogenic functions and therapeutic targeting of EphA2 in cancer. Oncogene *40*, 2483–2495. https://doi.org/10.1038/s41388-021-01714-8.
28. Wang, B., Liu, W., Liu, C., Du, K., Guo, Z., Zhang, G., Huang, Z., Lin, S., Cen, B., Tian, Y., et al. (2023). Cancer-Associated Fibroblasts Promote Radioresistance of Breast Cancer Cells via the HGF/c-Met Signaling Pathway. Int. J. Radiat. Oncol. Biol. Phys. *116*, 640–654. https://doi.org/10.1016/j.ijrobp.2022.12.029.
29. Yan, S., Jiao, X., Zou, H., and Li, K. (2015). Prognostic significance of c-Met in breast cancer: a meta-analysis of 6010 cases. Diagn. Pathol. *10*, 62. https://doi.org/10.1186/s13000-015-0296-y.
30. Lefebvre, C., and Allan, A.L. (2021). Anti-proliferative and anti-migratory effects of EGFR and c-Met tyrosine kinase inhibitors in triple negative breast cancer cells. Precis. Cancer Med. *4*, 2. https://doi.org/10.21037/pcm-20-62.
31. Eterno, V., Zambelli, A., Pavesi, L., Villani, L., Zanini, V., Petrolo, G., Manera, S., Tuscano, A., and Amato, A. (2014). Adipose-derived mesenchymal stem cells (ASCs) may favour breast cancer recurrence via HGF/c-Met signaling. Oncotarget *5*, 613–633.
32. Hughes, V.S., and Siemann, D.W. (2019). Failures in preclinical and clinical trials of c-Met inhibitors: evaluation of pathway activity as a promising selection criterion. Oncotarget *10*, 184–197. https://doi.org/10.18632/oncotarget.26546.
33. Miura, K., Wakayama, Y., Tanino, M., Orba, Y., Sawa, H., Hatakeyama, M., Tanaka, S., Sabe, H., and Mochizuki, N. (2013). Involvement of EphA2-mediated tyrosine phosphorylation

of Shp2 in Shp2-regulated activation of extracellular signal-regulated kinase. Oncogene *32*, 5292–5301. https://doi.org/10.1038/onc.2012.571.

34. Khatal, L., and More, H. (2019). Development and validation of a liquid chromatography-tandem mass spectrometry method for quantification of Lupeol in plasma and its application to pharmacokinetic study in rats. J. Chromatogr. B *1121*, 58–65. https://doi.org/10.1016/j.jchromb.2019.05.008.
35. Yousefi, M., Nosrati, R., Salmaninejad, A., Dehghani, S., Shahryari, A., and Saberi, A. (2018). Organ-specific metastasis of breast cancer: molecular and cellular mechanisms underlying lung metastasis. Cell. Oncol. *41*, 123–140. https://doi.org/10.1007/s13402-018-0376-6.
36. Neophytou, C., Boutsikos, P., and Papageorgis, P. (2018). Molecular Mechanisms and Emerging Therapeutic Targets of Triple-Negative Breast Cancer Metastasis. Front. Oncol. *8*, 31.
37. Ho-Yen, C.M., Jones, J.L., and Kermorgant, S. (2015). The clinical and functional significance of c-Met in breast cancer: a review. Breast Cancer Res. *17*, 52. https://doi.org/10.1186/s13058-015-0547-6.
38. Raghav, K.P., Wang, W., Liu, S., Chavez-MacGregor, M., Meng, X., Hortobagyi, G.N., Mills, G.B., Meric-Bernstam, F., Blumenschein, G.R., Jr., and Gonzalez-Angulo, A.M. (2012). cMET and Phospho-cMET Protein Levels in Breast Cancers and Survival Outcomes. Clin. Cancer Res. *18*, 2269–2277. https://doi.org/10.1158/1078-0432.CCR-11-2830.
39. Meta-analysis Group In Cancer, Piedbois, P., Rougier, P., Buyse, M., Pignon, J., Ryan, L., Hansen, R., Zee, B., Weinerman, B., Pater, J., et al. (1998). Efficacy of intravenous continuous infusion of fluorouracil compared with bolus administration in advanced colorectal cancer. J. Clin. Oncol. *16*, 301–308. https://doi.org/10.1200/JCO.1998.16.1.301.
40. Longley, D.B., Harkin, D.P., and Johnston, P.G. (2003). 5-fluorouracil: mechanisms of action and clinical strategies. Nat. Rev. Cancer *3*, 330–338. https://doi.org/10.1038/nrc1074.
41. Amstutz, U., Froehlich, T.K., and Largiadèr, C.R. (2011). Dihydropyrimidine dehydrogenase gene as a major predictor of severe 5-fluorouracil toxicity. Pharmacogenomics *12*, 1321–1336. https://doi.org/10.2217/pgs.11.72.
42. Del Mastro, L., Poggio, F., Blondeaux, E., De Placido, S., Giuliano, M., Forestieri, V., De Laurentiis, M., Gravina, A., Bisagni, G., Rimanti, A., et al. (2022). Fluorouracil and dose-dense adjuvant chemotherapy in patients with early-stage breast cancer (GIM2): end-of-study results from a randomised, phase 3 trial. Lancet Oncol. *23*, 1571–1582. https://doi.org/10.1016/S1470-2045(22)00632-5.
43. Ferguson, J.E., and Orlando, R.A. (2015). Curcumin reduces cytotoxicity of 5-Fluorouracil treatment in human breast cancer cells. J. Med. Food *18*, 497–502. https://doi.org/10.1089/jmf.2013.0086.
44. Scagliotti, A., Capizzi, L., Cazzaniga, M.E., Ilari, A., De Giorgi, M., Cordani, N., Gallazzi, M., Bruno, A., Pelosi, G., Albini, A., et al. (2022). Co-targeting triple-negative breast cancer cells and endothelial cells by metronomic chemotherapy inhibits cell regrowth and migration via downregulation of the FAK/VEGFR2/VEGF axis and autophagy/apoptosis activation. Front. Oncol. *12*, 998274. https://doi.org/10.3389/fonc.2022.998274.
45. Gjerdrum, C., Tiron, C., Høiby, T., Stefansson, I., Haugen, H., Sandal, T., Collett, K., Li, S., McCormack, E., Gjertsen, B.T., et al. (2010). Axl is an essential epithelial-to-mesenchymal transition-induced regulator of breast cancer metastasis and patient survival. Proc. Natl. Acad. Sci. USA *107*, 1124–1129. https://doi.org/10.1073/pnas.0909333107.
46. Chen, J., Lu, L., Feng, Y., Wang, H., Dai, L., Li, Y., and Zhang, P. (2011). PKD2 mediates multi-drug resistance in breast cancer cells through modulation of P-glycoprotein expression. Cancer Lett. *300*, 48–56. https://doi.org/10.1016/j.canlet.2010.09.005.
47. Cháirez-Ramírez, M.H., Gallegos-Infante, J.A., Moreno-Jiménez, M.R., González-Laredo, R.F., and Rocha-Guzmán, N.E. (2019). Absorption and distribution of lupeol in CD-1 mice evaluated by UPLC–APCI+–MS/MS. Biomed. Chromatogr. *33*, e4432. https://doi.org/10.1002/bmc.4432.
48. Wang, Z., Wang, Y., Yu, T., Hu, Z., and Wang, Y. (2021). An LC-ESI/MS/MS method for the determination of lupeol via precolumn derivatization and its application to pharmacokinetic studies in rat plasma. Biomed. Chromatogr. *35*, e5005. https://doi.org/10.1002/bmc.5005.
49. Ganaie, A.A., Siddique, H.R., Sheikh, I.A., Parray, A., Wang, L., Panyam, J., Villalta, P.W., Deng, Y., Konety, B.R., and Saleem, M. (2020). A novel terpenoid class for prevention and treatment of KRAS-driven cancers: Comprehensive analysis using *in situ*, *in vitro*, and *in vivo* model systems. Mol. Carcinog. *59*, 886–896. https://doi.org/10.1002/mc.23200.
50. Xu, Y., Li, Q., Li, X.-Y., Yang, Q.-Y., Xu, W.-W., and Liu, G.-L. (2012). Short-term anti-vascular endothelial growth factor treatment elicits vasculogenic mimicry formation of tumors to accelerate metastasis. J. Exp. Clin. Cancer Res. *31*, 16. https://doi.org/10.1186/1756-9966-31-16.
51. A tissue-engineered 3D microvessel model reveals the dynamics of mosaic vessel formation in breast cancer. PMC. https://www.ncbi.nlm.nih.gov/pmc/articles/PMC7541732/.
52. Maniotis, A.J., Folberg, R., Hess, A., Seftor, E.A., Gardner, L.M., Pe'er, J., Trent, J.M., Meltzer, P.S., and Hendrix, M.J. (1999). Vascular Channel Formation by Human Melanoma Cells in Vivo and in Vitro: Vasculogenic Mimicry. Am. J. Pathol. *155*, 739–752.
53. Zudaire, E., Gambardella, L., Kurcz, C., and Vermeren, S. (2011). A computational tool for quantitative analysis of vascular networks. PLoS One *6*, e27385. https://doi.org/10.1371/journal.pone.0027385.
54. Duarte, D., and Vale, N. (2022). Evaluation of synergism in drug combinations and reference models for future orientations in oncology. Curr. Res. Pharmacol. Drug Discov. *3*, 100110. https://doi.org/10.1016/j.crphar.2022.100110.
55. Majumder, B., Baraneedharan, U., Thiyagarajan, S., Radhakrishnan, P., Narasimhan, H., Dhandapani, M., Brijwani, N., Pinto, D.D., Prasath, A., Shanthappa, B.U., et al. (2015). Predicting clinical response to anticancer drugs using an ex vivo platform that captures tumour heterogeneity. Nat. Commun. *6*, 6169. https://doi.org/10.1038/ncomms7169.
56. Brantley-Sieders, D.M., Fang, W.B., Hicks, D.J., Zhuang, G., Shyr, Y., and Chen, J. (2005). Impaired tumor microenvironment in EphA2-deficient mice inhibits tumor angiogenesis and metastatic progression. Faseb. J. *19*, 1884–1886. https://doi.org/10.1096/fj.05-4038fje.
57. Tandon, M., Vemula, S.V., and Mittal, S.K. (2011). Emerging strategies for EphA2 receptor targeting for cancer therapeutics. Expert Opin. Ther. Targets *15*, 31–51. https://doi.org/10.1517/14728222.2011.538682.
58. Coxon, A., Rex, K., Meyer, S., Sun, J., Sun, J., Chen, Q., Radinsky, R., Kendall, R., and Burgess, T.L. (2009). Soluble c-Met receptors inhibit phosphorylation of c-Met and growth of hepatocyte growth factor: c-Met-dependent tumors in animal models. Mol. Cancer Ther. *8*, 1119–1125. https://doi.org/10.1158/1535-7163.MCT-08-1032.
59. Cashman, R., Cohen, H., Ben-Hamo, R., Zilberberg, A., and Efroni, S. (2014). SENP5 mediates breast cancer invasion via a TGFβRI SUMOylation cascade. Oncotarget *5*, 1071–1082.
60. Dasgupta, S., Ghosh, T., Dhar, J., Bhuniya, A., Nandi, P., Das, A., Saha, A., Das, J., Guha, I., Banerjee, S., et al. (2021). RGS5-TGFβ-Smad2/3 axis switches pro- to anti-apoptotic signaling in tumor-residing pericytes, assisting tumor growth. Cell Death Differ. *28*, 3052–3076. https://doi.org/10.1038/s41418-021-00801-3.
61. Amato, K.R., Wang, S., Tan, L., Hastings, A.K., Song, W., Lovly, C.M., Meador, C.B., Ye, F., Lu, P., Balko, J.M., et al. (2016). EPHA2 blockade overcomes acquired resistance to EGFR kinase inhibitors in lung cancer. Cancer Res. *76*, 305–318. https://doi.org/10.1158/0008-5472.CAN-15-0717.
62. Sameni, M., Tovar, E.A., Essenburg, C.J., Chalasani, A., Linklater, E.S., Borgman, A., Cherba, D.M., Anbalagan, A., Winn, M.E., Graveel, C.R., and Sloane, B.F. (2016). Cabozantinib (XL184) Inhibits Growth and Invasion of Preclinical TNBC Models. Clin. Cancer Res. *22*, 923–934. https://doi.org/10.1158/1078-0432.CCR-15-0187.
63. Kawase, N., Sugihara, A., Kajiwara, K., Hiroshima, M., Akamatsu, K., Nada, S., Matsumoto, K., Ueda, M., and Okada, M. (2022). SRC kinase activator CDCP1 promotes hepatocyte growth factor–induced cell migration/invasion of a subset of breast cancer cells. J. Biol. Chem. *298*, 101630. https://doi.org/10.1016/j.jbc.2022.101630.
64. Saha, D., Mitra, D., Alam, N., Sen, S., Mustafi, S.M., Majumder, P.K., Majumder, B., and Murmu, N. (2023). Lupeol and Paclitaxel cooperate in hindering hypoxia induced vasculogenic mimicry via suppression of HIF-1α-EphA2-Laminin-5γ2 network in human oral cancer. J. Cell Commun. Signal. *17*, 591–608. https://doi.org/10.1007/s12079-022-00693-z.
65. Tao, K., Fang, M., Alroy, J., and Sahagian, G.G. (2008). Imagable 4T1 model for the study of late stage breast cancer. BMC Cancer *8*, 228. https://doi.org/10.1186/1471-2407-8-228.
66. Bello-Monroy, O., Mata-Espinosa, D., Enríquez-Cortina, C., Souza, V., Miranda, R.U., Bucio, L., Barrios-Payán, J., Marquina-Castillo, B., Rodríguez-Ochoa, I., Rosales, P., et al. (2020). Hepatocyte growth factor enhances the clearance of a multidrug-resistant Mycobacterium tuberculosis strain

by high doses of conventional chemotherapy, preserving liver function. J. Cell. Physiol. *235*, 1637–1648. https://doi.org/10.1002/jcp.29082.

67. Zhang, X., Gao, Z., Chen, K., Zhuo, Q., Chen, M., Wang, J., Lai, X., and Wang, L. (2022). Lupeol inhibits the proliferation and migration of MDA-MB-231 breast cancer cells via a novel crosstalk mechanism between autophagy and the EMT. Food Funct. *13*, 4967–4976. https://doi.org/10.1039/D2FO00483F.
68. Ghosh, S., Pal, A., and Ray, M. (2019). Methylglyoxal in combination with 5-Fluorouracil elicits improved chemosensitivity in breast cancer through apoptosis and cell cycle inhibition. Biomed. Pharmacother. *114*, 108855. https://doi.org/10.1016/j.biopha.2019.108855.
69. Chou, T.-C. (2010). Drug combination studies and their synergy quantification using the Chou-Talalay method. Cancer Res. *70*, 440–446. https://doi.org/10.1158/0008-5472.CAN-09-1947.
70. Chou, T.C., and Talalay, P. (1984). Quantitative analysis of dose-effect relationships: the combined effects of multiple drugs or enzyme inhibitors. Adv. Enzyme Regul. *22*, 27–55. https://doi.org/10.1016/0065-2571(84)90007-4.
71. Chou, T.-C., and Talalay, P. (1983). Analysis of combined drug effects: a new look at a very old problem. Trends Pharmacol. Sci. *4*, 450–454. https://doi.org/10.1016/0165-6147(83)90490-X.

STAR★METHODS

KEY RESOURCES TABLE

REAGENT or RESOURCE	SOURCE	IDENTIFIER
Antibodies		
Rabbit polyclonal Anti-human/mouse Ki67	Affinity Biosciences	Cat# AF0198; RRID: AB_2834152
Rabbit Anti-human/mouse Cleaved-Caspase 3 (Asp175), p17	Affinity Biosciences	Cat# AF7022; RRID: AB_2835326
Rabbit polyclonal Anti human/mouse MET (C-28)	Santa Cruz Biotechnology	Cat# sc-161; RRID: AB_631941
Rabbit polyclonal Anti human/mouse p-MET (Tyr 1349)	Santa Cruz Biotechnology	Cat# sc-34086; RRID: AB_2144033
Rabbit Anti human/mouse EphA2 (D4A2)	Cell Signaling Technology	Cat#6997; RRID: AB_10827743
Rabbit Anti human/mouse Phospho-EphA2 (Ser897) (D9A1)	Cell Signaling Technology	Cat#6347; RRID: AB_11220420
Rabbit Anti human/mouse Phospho-p44/42 MAPK (Erk1/2) (Thr202/Tyr204) (D13.14.4E) XP	Cell Signaling Technology	Cat#4370; RRID: AB_2315112
Mouse Anti human/mouse MMP-2 (clone 8B4)	Novus	Cat# NB200-114; RRID: AB_350369
mouse Anti human Laminin- 5 (Y2 chain) (D4B5)	Millipore	Cat#MAB19562; RRID: AB_94454
Rabbit polyclonal anti -Bcl2, unconjugated	Novus Biologicals	Cat# NB100-56101; RRID: AB_2064432
mouse monoclonal anti-Bax (Clone: B9)	Santa Cruz Biotechnology	Cat # sc-7480; RRID: AB_626729
Rabbit polyclonal Anti E-cadherin (H-108)	Santa Cruz Biotechnology	Cat# sc-7870; RRID: AB_2076666
Mouse monoclonal Anti human Vimentin (V9)	Santa Cruz Biotechnology	Cat# sc-6260; RRID: AB_628437
Rabbit polyclonal Anti- human ERK1+ERK2 antibody	Abcam	Cat# ab17942; RRID: AB_2297336
Mouse anti human/mouse Twist-1 (10E4E6)	Novus	Cat# NBP2-37364; RRID: AB_2801339
Mouse monoclonal anti human slug (4B6D5)	Thermo Fisher Scientific	Cat# MA5-38634; RRID: AB_2898546
Mouse Anti human Snail1 (20C8)	Thermo Fisher Scientific	Cat# 14-9859-82; RRID: AB_2573045
Goat Anti-Rabbit IgG (H+L) Secondary Antibody, HRP	Thermo Fisher Scientific	Cat# 31460; RRID: AB_228341
Rabbit anti-Mouse IgG (H+L) Secondary Antibody, HRP.	Thermo Fisher Scientific	Cat# # 61-6520; RRID: AB_2533933
Biological samples		
Human CaBr tumor material	Chittaranjan National Cancer Institute, Hospital wing	Collected per A-4.311/NM/26/11/2018
Chemicals, peptides, and recombinant proteins		
Fetal Bovine serum	Gibco	Cat# 10438026
0.25% Trypsin-EDTA (1X)	Gibco	Cat# 25200072
Dulbecco's Modified Eagle Medium powder	Gibco	Cat# 12800017
RPMI Medium 1640	Gibco	Cat# 31800022
Anti-Anti (100X)	Gibco	Cat# 15240062
Matrigel Matrix Basement Membrane, Growth Factor Reduced, Phenol red free	Corning	Cat# 356231
MTT	Merck	Cat# 475989
Dimethyl Sulfoxide	Sigma	Cat# D2650
Gram's crystal violet solution	Merck	Cat# 10921801251730
Insulin solution from bovine pancreas	Sigma	Cat# I0516
Formaldehyde solution	Merck	Cat# 1.94900.0521
Lupeol	Sigma-Aldrich	Cat# S957712
5FU	Sigma-Aldrich	Cat# F6627
4-hydroperoxy cyclophosphamide	Cayman	Cat#19527
Epirubicin Hydrochloride	BioVision	Cat# 1753
Docetaxel	BioVision	Cat# 2232

(*Continued on next page*)

Continued

REAGENT or RESOURCE	SOURCE	IDENTIFIER
Doxorubicin.HCL	BioVision	Cat#1527
Paclitaxel	Sigma-Aldrich	Cat#T1912
Human HGF	Sigma-Aldrich	Cat# H9661
Recombinant mouse HGF protein	R&D Systems	Cat# 2207-HG-025/CF
B-27™ Supplement (50X), serum free	Gibco	Cat# 17504044
ALW-II-41-27	Cayman	Cat# 1186206-79-0
Cabozantinib	APExBIO	Cat# A2977
XenoLight D-Luciferin, Potassium salt	Perkin-Elmer	Cat# 122799
Critical commercial assays		
jetPRIME Transfection Reagent	Polyplus	Cat# 11407
In vivo-jetPEI	Polyplus	Cat# 201
IHC Select, Immunoperoxidase Secondary Detection System	Millipore	Cat# DAB150
Annexin V Apoptosis Detection Kit	Santa Cruz	Cat# sc-4252 AK
Experimental models: Cell lines		
MDA MB 231	NCCS, Pune, India	
4T1		Kindly gifted by Dr. Rathindranath Baral (CNCI, India)
Experimental models: Organisms/strains		
BALB/c (Female)	State Centre for Laboratory Animal Breeding, West Bengal Livestock Development Corporation Limited	
Oligonucleotides		
ON-TARGET plus Human MET (4233) siRNA- SMARTpool	Dharmacon	Cat# L-003156-00-0005
ON-TARGETplus Human EphA2 (1969) siRNA-SMARTpool	Dharmacon	Cat# L-003116-00-0005
ON-TARGET plus Mouse Met (17295) siRNA- SMARTpool	Dharmacon	Cat# L-040878-00-0005
ON-TARGET plus Mouse EphA2 (13836) siRNA- SMARTpool	Dharmacon	Cat# L-040412-00-0005
ON-TARGETplus Non-targeting Pool	Dharmacon	Cat# D-001810-10-05
Software and algorithms		
FlowJo 10.8.1	BD Biosciences	
GraphPad Prism 7.0	GraphPad software Inc.	
SPSS	SPSS Inc.	
Fiji	ImageJ	
AngioTool v0.6a		Zudaire et al.[53]
SynergyFinder 3.0		Ianevski et al.[54]

RESOURCE AVAILABILITY

Lead contact

Additional information and any request for resources or materials should be directed to and will be fulfilled by the lead contact, Dr. Nabendu Murmu (nabendu.murmu@cnci.ac.in).

Materials availability

This study did not generate new unique reagents.

Data and code availability

- Data: All data generated or analyzed during this study are included in this published article. All relevant data are available from the lead contact upon request.
- Code: This paper does not report original code.
- Any additional information required to reanalyze the data reported in this paper is available from the lead contact upon request.

EXPERIMENTAL MODEL AND STUDY PARTICIPANT DETAILS

Patients and samples

Retrospective clinicopathological and survival data of 135 patients with triple-negative breast cancer (TNBC) were collected from the epidemiology department of the Chittaranjan National Cancer Institute, Kolkata. All relevant patient data were collected and anonymized prior to the analysis. The actual screening method, along with the exclusion and inclusion criteria during patient selection, is shown in Figure S1. Formalin-fixed paraffin-embedded (FFPE) blocks containing recurrent cancerous tissue were collected for future use. Also, fresh TNBC tissues were collected in three phases (N= 15, N=10 and N=7), which were then utilized for patient-derived *ex vivo* explant cultures. **Informed patient consent was obtained. This study was approved by the Institute Ethical Committee having the approval number: A-4.311/NM/26/11/2018** and the Declaration of Helsinki ethical standards and its later amendments were strictly adhered to. **The patients included in this study are of South Asian ancestry.**

Cell lines and reagents

The TNBC cell line MDA-MB-231was procured from NCCS, Pune (INDIA). The murine TNBC cell line 4T1(containing stable expression of the luc2 gene) was a gift from Dr. Rathindranath Baral, Department of Immunoregulation and Immunodiagnostics, Chittaranjan National Cancer Institute, Kolkata. MDA-MB-231 and 4T1 cells were cultured in DMEM containing high glucose and RPMI 1640 media (Gibco, Life Technologies, USA) respectively. The medium was supplemented with 10% FBS (Gibco, Life Technologies, USA) and 1% penicillin-streptomycin (Gibco, Life Technologies, USA) and the cells were maintained in a humidified incubator at 37°C with a constant 5% carbon dioxide environment. Purified Lupeol (S957712), 5- Fluorouracil (5FU) (F6627), human HGF (H9661) from Sigma Aldrich, and recombinant mouse HGF protein (2207-HG-025/CF, R&D Systems) were used for further experiments.

Mice

Female BALB/c (4-6 weeks old) mice were purchased from State Centre for Laboratory Animal Breeding, West Bengal Livestock Development Corporation Limited, India. **All mice were cared for in accordance with the ethical guidelines and rules set and overseen by the Committee for the purpose of control and supervision of experiments on animals (CPCSEA), India. Protocols used for animal studies were reviewed and approved by the Institutional animal ethics committee having the approval number IAEC-1774/NM-18/2021/17.**

METHOD DETAILS

Patient cohort stratification and follow-up

The TNBC patient cohort (N=135) (Table S1) was then stratified into two groups based on the adjuvant therapy they received. One group received 5- Fluorouracil (5FU) containing standard of care (SOC) (5FU, Epirubicin and Cyclophosphamide), and the other group received SOC without 5FU (Doxorubicin, Docetaxel and Cyclophosphamide or Paclitaxel). After a follow-up period of 5 years, cases of recurrence were recorded, and Kaplan-Meier survival plots for disease-free survival (DFS) were prepared. Of the 45 (33.33%) recurrent cases, 35 archived formalin-fixed paraffin-embedded (FFPE) blocks containing recurrent cancerous tissue were collected for future use.

Ex vivo tumor fragment culture

Fresh TNBC tissues were collected in three phases (N= 15, N=10 and N=7), which were then utilized for patient-derived *ex vivo* explant cultures as performed earlier.[55] The tissues were sliced into 3 mm^3 pieces and cultured in RPMI 1640 medium (Gibco, Life Technologies, USA) containing 8% FBS or HGF and 2% autologous serum. 5FU, Lupeol alone or in combination and also standards of care (Epirubicin+ Cyclophosphamide+ 5FU; Doxorubicin+ Docetaxel+ Cyclophosphamide; Doxorubicin+ Cyclophosphamide+ Paclitaxel) were added to the treatment arms and incubated for 48 h at 37°C in a 5% CO2 atmosphere on an orbital shaker at 20 rpm. **The C_{max} of the SOCs are as follows: Epirubicin= 9μg/ml; Cyclophosphamide= 10μM; 5FU= 16μg/ml; Doxorubicin= 1μg/ml; Docetaxel= 2μg/ml; Paclitaxel= 7μM.** Each patient's healthcare records were consulted to gather pertinent clinicopathological and demographic data (Tables S2 and S9).

Immunohistochemistry staining

Tumor slices were fixed in 10% buffered formalin, and formalin-fixed paraffin-embedded (FFPE) blocks were prepared after 24 h of fixation. FFPE blocks were sectioned (4μm) and immunohistochemical (IHC) staining was performed using an IHC kit (DAB 150, Merck) following the manufacturer's protocol. The slides were visualized under a bright-field microscope (Carl Zeiss), and images were captured using Zen software. IHC Scoring was performed as previously described.[19]

siRNA mediated silencing

c-MET and EphA2 are over-expressed in both the MDA-MB-231 and 4T1 cells.[30–32,56–58] siRNAs targeting the human c-MET (ON-TARGET plus Human MET (4233) siRNA- SMARTpool, cat# L-003156-00-0005) and human EphA2 (ON-TARGETplus Human EphA2 (1969) siRNA-SMARTpool, cat# L-003116-00-0005) genes were purchased from Dharmacon (Lafayette, CO, USA). In addition, siRNAs targeting Mouse Met (ON-TARGET plus Mouse Met (17295) siRNA- SMARTpool, ca# L-040878-00-0005) and Mouse EphA2(ON-TARGET plus Mouse EphA2 (13836) siRNA- SMARTpool, cat# L-040412-00-0005) were obtained. A non-targeting pool (NTP) (ON-TARGETplus Non-targeting Pool, cat# D-001810-10-05) was used as the negative control. *In vitro* JetPRIME transfection reagent (Polyplus) was used to transfect these siRNAs individually or simultaneously into MDA-MB-231 and 4T1 cells, according to the manufacturer's protocol.[59] Western blot analysis was performed to confirm the knockdown. Various concentrations of siRNAs were transfected, and the concentration that achieved maximum silencing was used for further experiments.

In vivo intra-tumoral knockdown was performed by combining siRNAs (10μg) targeting murine EphA2 and MET with *in vivo*-jet PEI (1.2μl) and 5% solution of Sucrose (50μl).[60] Initial delivery was performed when the tumor volume reached approximately 40–60 mm^2. Four doses of siRNAs were given to each mouse every other day and were sacrificed 3 days after the last injection.

Pharmacological regulation

ALW-II-41-27 (0.5μM)[61] and Cabozantinib (2 μM)[62] was used as specific pharmacological phosphorylation inhibitors targeting EphA2 and c-MET respectively. HGF (100ng/ml)[63] was applied to cells for 15 min prior to the experimental endpoint. Western blot analysis was performed to confirm inhibition/activation.

Western blotting

Western blotting was performed as previously described.[64] Total cell lysates (50 μg) were resolved by SDS-PAGE and transferred to Polyvinyldene di-fluoride (PVDF) membrane by semi-dry electroblotting (BIO-RAD). After non-specific protein blocking with 5% non-fat dry milk for 1 h at room temperature, the membranes were incubated with primary antibodies overnight at 4°C followed by incubation with appropriate horseradish peroxidase (HRP) tagged secondary antibodies for 1 h at room temperature. The protein bands were visualized using ECL (BIO-RAD) and captured in a ChemiDoc XRS (BIO-RAD) using Image Lab software (Bio-RAD), followed by densitomentric analysis using ImageJ software. β-actin was used as a loading control.

Transwell invasion and migration

Transwell inserts (Corning) with a pore size of 8 μm were used in this experiment. The inserts were coated with growth factor-reduced Matrigel (Corning) for the invasion assays. Transfected and knocked down MDA-MB-231 cells ($1x10^5$) were initially seeded into Transwell inserts containing serum-free media. Pharmacological inhibitors, Lupeol, 5FU or both were also added to the respective inserts. The lower chamber contained media containing HGF (100 ng/ml), which acts as a chemotactic factor. After incubation for 48 h, the inserts were collected. The migrated and invaded cells present on the lower side of the insert were fixed in methanol, stained with crystal violet, and visualized using a bright-field microscope (Carl Zeiss).

Mammosphere formation assay

MDA-MB-231 cells ($1x10^3$) were seeded into each well of ultra-low attachment 96 well plates in mammosphere forming media (serum-free DMEM high glucose media with100 ng/ml HGF, 1X B27 supplement and 5μg/ml Insulin). Post-transfection and knockdown with pharmacological inhibitors, single agent Lupeol, 5FU or both in combination were added. The plates were incubated for 7 days without any disturbance, and the formed mammospheres were observed. The primary mammospheres were dissociated, and single cells were subsequently seeded for evaluation of secondary mammosphere formation and further incubated for a week. Images were obtained using an inverted light microscope (Olympus).

Tube formation assay

Each well of a 96 well plate was coated with growth factor-reduced matrigel. A total of $1x10^3$transfected and knocked downMDA-MB-231 cells were seeded in each coated well. HGF, pharmacological inhibitors, Lupeol, 5FU, or both were added to the respective wells and incubated for 3 days to observe their effect on the tube-forming capability of the cells. The tubes were then visualized under an inverted light microscope (Olympus). AngioTool v0.6a software[53] was used to quantify the total vessel length and number of junctions in the tubes formed in various groups.

In vivo experiments

Initially, siRNA-mediated c-MET, EphA2, or dual knockdown 4T1 cells ($1x10^6$) were injected into the abdominal mammary fat pads of BALB/c mice, following a previously described protocol.[65] Tumor growth was observed every other day by injecting the mice with XenoLight D-Luciferin, Potassium salt (Product no.:122799, Perkin Elmer). *In vivo* live animal imaging was performed using an IVIS Lumina *in vivo* imaging system (PerkinElmer). From the 5^{th} day, the mice in all groups except the control group were treated with mouse HGF (10μg/g/week).[66] At ethical endpoints, the mice were sacrificed and the tumors were harvested. Similar regimens were followed for combinatorial studies, with

Lupeol (20 mg/kg/2 days) (intraperitoneal)[67] and/or 5FU (10 mg/kg/2 days)[68] (intraperitoneal), as well as mouse HGF. In addition, initial cytotoxicity studies with the above-mentioned treatment regimens were conducted in non-tumor-bearing BALB/c mice.

Cytotoxicity assay

Cellular cytotoxicity was evaluated using an MTT colorimetric assay after 24 h of treatment. $1x10^3$ MDA-MB-231 cells/well were plated in 96 well plates containing complete medium and allowed to adhere for 24 hours. Subsequently, the medium was replaced with fresh complete medium containing various doses of 5FU and Lupeol. After 24 h of incubation, 10μl MTT (stock concentration: 2mg/ml) was added to each well. The plates were then incubated at 37°C for 4 h. The formazan crystals formed were solubilized in 100% DMSO. Absorbance was measured using a multi-mode plate reader at 570nm. The GraphPad Prism software (version 7.0) was used to calculate the IC_{50}value of each compound. Based on these values, an MTT assay was performed to evaluate the combinatorial effect of Lupeol and 5FU using sub-IC_{50} doses of both compounds.

Determination of combination effect

The online tool "SynergyFinder 3.0" was utilized to compute the dose response heat map and the synergy distribution (Bliss synergy score; mean) for the combination of 5FU and Lupeol.[54] Also, the combination index (CI) was determined according to the method described by Chou and Talalay.[69] Briefly, MDA-MB-231 cells ($1x10^3$) were plated and subsequently treated for 24 h in the presence or absence of1) Lupeol (0-180 μM), 2) 5FU (0-170 μM), and 3) 5FU (0-15 μM) + Lupeol (0-20 μM). The IC_{50} values for various treatments were calculated, and the concentration of each component required to reduce the viability to 50% was used to compute the CI. For the effect of the combination of the two drugs, the CI values of 0.9 were judged to be synergistic, CI between 0.9-1.1 considered to be additive, and >1.1 was antagonistic.[70,71] For all further *in vitro* experiments involving Lupeol and 5FU, the respective doses of 8μM and 10μM were used.

Colony formation assay

MDA-MB-231 cells were plated in 6 well plates at low densities (250 cells/ well) and incubated at 37°C overnight. The cells were then treated with Lupeol or 5FU alone or in combination in serum free media with/without HGF. The cells were incubated for 24 hours, then the media was changed, and the cells were incubated for further 7 days. The colonies that formed (>50 cells) were fixed in 100% cold methanol and stained with 0.5% crystal violet and visualized under an inverted bright field microscope (Olympus).

Wound healing assay

MDA-MB-231 cells were plated in 6 well plates in serum containing media and monitored till they reached high confluency. A scratch was made using a 200 μl sterile tip and the media was replaced by serum free media containing Lupeol, 5FU alone or both and/or HGF. The cellular wound healing capacity was monitored every 24 hours. The end point for this experiment was when the cells completely healed the inflicted wound. Imaging was done using an inverted light microscope (Olympus). The total wound area was quantified using ImageJ software.

Apoptosis assay

MDA-MB-231 cells were plated in 6 well plates in serum containing media and allowed to adhere overnight. Then, the media was replaced with serum free media. The cells were treated with HGF, 5FU, Lupeol alone or in combination. After 24 hours of treatment, the cells were used for performing the apoptosis assay using the Annexin V/PI kit (Santa Cruz) following the manufacturer's protocol. Briefly, the cells were washed with PBS and 5 μl of FITC tagged Annexin V and 3 μl of PI was added and incubated in dark conditions at room temperature (RT) for 15 mins. The cells acquired immediately by flow cytometry using FACSCalibur instrument (BD). Data was analyzed using FlowJo software.

Immunofluorescence staining

Immunofluorescence staining was performed as previously described.[22] MDA-MB-231 cells were cultured in sterile glass cover slips. Post-treatment with HGF, 5FU and/or Lupeol, the cells were exposed to respective primary and secondary antibodies and fixed with Methanol. The cells were visualized under a fluorescence microscope (OLYMPUS). ImageJ software was used to calculate the corrected total cell fluorescence. The primary antibodies used were rabbit polyclonal anti-Bax (clone B9; 1:200 dilution, Santa Cruz Biotechnology), rabbit polyclonal anti-E-cadherin (clone H-108; 1:200 dilution; Santa Cruz Biotechnology) and mouse monoclonal anti-Vimentin (clone V9; 1:200 dilution; Santa Cruz Biotechnology). The secondary antibodies used in this experiment were goat anti-rabbit IgG F(ab')2 secondary antibody conjugated with FITC (1:500 dilution) and F(ab')2 goat anti-mouse IgG (H+L) secondary antibody conjugated with PE (1:500 dilution).

Protein-protein interaction (PPI) analysis and network modeling

All input markers were chosen from the current study and queried using STRING protein-protein interaction (PPI) network analysis (https://string-db.org) *in silico* using a combination of text mining, databases, experiments, co-expression, neighborhood, gene fusion, co-occurrence, full network (type), confidence (edge meaning), and multiple active interaction sources and channels. A high-confidence (edge) interaction score of 0.700was chosen as the minimum requirement, and edges with a confidence of 0.700 or above were considered as the highest.

No additional layer or second shell was created. Instead, we confined the maximum number of interaction scores to only the input proteins whose roles were elucidated and profiled within the framework of the present study.

QUANTIFICATION AND STATISTICAL ANALYSIS

Each experiment was performed in triplicate. GraphPad Prism software version 7.0 was used for all statistical analyses, and data are represented as mean ±SD (Intuitive Software for Science, San Diego, CA, USA). Chi-square test and one- or two-way ANOVA ($p < 0.05$) were used to compare all of the studies, followed by post-tests using Bonferroni or Tukey's test. Survival curves were computed by the Kaplan–Meier method and the differences in survival time (months) was compared using the Log-rank test. These statistical analyses were conducted using the SPSS 17 software (SPSS Inc, Chicago, IL, USA). p value less than 0.05 was considered to be significant.